Xrn1 influences RNA pol II-dependent transcription elongation rates across the yeast genome and this control is particularly relevant for late elongation of regulatory genes.

Victoria Begley[1,6], Antonio Jordán-Pla[2,6], Xenia Peñate[1], Ana I. Garrido-Godino[3], Drice Challal[4], Abel Cuevas-Bermúdez[3], Adrià Mitjavila[1], Mara Barucco[4], Gabriel Gutiérrez[1], Abhyudai Singh[5], Paula Alepuz[2], Francisco Navarro[3], Domenico Libri[4,7], José E. Pérez-Ortín[2,7] and Sebastián Chávez[1,7].

[1] Instituto de Biomedicina de Sevilla, Universidad de Sevilla-CSIC-Hospital Universitario V. del Rocío, Seville, 41012, Spain.

[2] E.R.I. Biotecmed, Universitat de València; Burjassot, Valencia, 46100, Spain.

[3] Departamento de Biología Experimental, Facultad de Ciencias Experimentales, Universidad de Jaén, Jaén, 23071, Spain.

[4] Institut Jacques Monod, Centre National de la Recherche Scientifique, UMR 7592, Université Paris Diderot, Sorbonne Paris Cité, 75205 Paris, France.

[5] Department of Electrical and Computer Engineering, University of Delaware, Newark, DE 19716, USA

[#]Present Address

Victoria Begley, UCL Cancer Institute, University College London, 72 Huntley Street, London WC1E 6BT, UK.

[6] These authors contribute equally to this work

[7] Joint senior authors

* To whom correspondence should be addressed: schavez@us.es

Keywords: Transcription elongation, mRNA decay, Xrn1, 3' pre-mRNA processing

Abstract

mRNA homeostasis is favored by crosstalks between transcription and degradation machineries. This involves co-transcriptional modulation of mRNA decay by molecular imprinting, and feedback regulation of transcription by degradation factors. Both the Ccr4-NOT and the Xrn1-decaysome complexes have been described to influence transcription. While Ccr4-NOT has been shown to directly stimulate transcription elongation, the information available on how Xrn1 influences transcription is scarce and, in some cases, contradictory. In this study we have addressed this issue by mapping RNA polymerase II (RNApol II) at high resolution, using CRAC and BioGRO-seq techniques in *Saccharomyces cerevisiae*. We found significant effects of Xrn1 perturbation on RNA pol II profiles across the genome, in both the 5' and 3' ends of gene bodies. Downstream of the transcription start site, RNA pol II profiles exhibited significant reductions in slope that were compatible with decreased elongation rates. This phenomenon was also observed soon after the nuclear pool of Xrn1 was depleted. Nucleosome mapping confirmed drastically altered chromatin dynamics during early elongation. We also found an accumulation of arrested RNApol II at the 3' end, immediately upstream of polyadenylation sites of most genes, with particular incidence in those genes functionally related to regulatory processes. Lack of Xrn1 provoked alterations in RNApol II CTD phosphorylation and increased recruitment of 3' pre-mRNA processing factors. However, accumulation of RNApol II at 3' ends was rather related to the nucleosomal configuration of those regions. We conclude that Xrn1 influences RNA pol II-dependent transcription elongation and this control is particularly relevant for genes with a certain type of chromatin structure at 3'.

Introduction

The dynamic equilibrium that keeps mRNA concentration is a balance between synthesis and degradation processes. In the classic paradigm, the 'central dogma' of molecular biology is a linear path in which the mRNA plays a role as an intermediary between genes and proteins. In the recent years our team has helped to demonstrate

that there is a general control of the total cellular concentration of mRNA ([mRNA] homeostasis) in the yeast *Saccharomyces cerevisiae* and that it is the result of the crosstalk between transcription and degradation machineries (mRNA-crosstalk) [1]. This involves both the mRNA imprinting by RNA binding proteins or base methylation, during its synthesis [2], as well as the feedback on the transcription machinery exercised by the decaysome [1]. Other authors have demonstrated the existence of additional cross-talk mechanisms in this yeast dependent on the Ccr4-NOT complex [3] or on the Nab2 mRNA binding protein [4]. There are also evidences of the existence of transcription-degradation cross-talk in human cells for a subset of mRNAs through the Ccr4–Not and Xrn1 complexes [5, 43] and during viral infections [6]. In fact, for several of these complexes it has been demonstrated that there is also an extended connection to translation of the imprinted mRNAs. Both the Ccr4-NOT (7) and the Xrn1 (decaysome) complexes (8) have a positive role on the translation of certain mRNAs that were, presumably, previously imprinted by them during transcription. This points to the existence of a transcription-translation cross-talk as well.

RNA pol II transcription is traditionally divided into three phases (20): i) the formation of the PIC (pre-initiation complex) that requires the successive binding of a plethora of factors over the basal promotor sequences; ii) the elongation phase after the escape of RNA pol II, and associated factors, from the promoter while synthesizing the mRNA; and iii) the termination phase that is composed by a polyadenylation/cleavage step of the primary transcript and a release of the downstream RNA pol by the concerted action of pause sequences and the activity of the Rat1 (Xrn2) exonuclease (see refs. 41,46 for a review).

After initiation, some auxiliary factors remain bound to the basal promoter and some others travel with RNA pol II and a new set of factors that are required for fast and accurate elongation (25-26, 35). For instance, lack of the elongation factor TFIIS provokes increased levels of backtracked RNA pol II (27) and specific defects in RP genes (28). The elongation of RNA pol II through chromatin is influenced by the nucleosomal organization and specific histone modifications of each gene (42) and, at the same time, elongation affects both nucleosome positions and histone marks (42). There is a continuous cross-talk between the elongating complex and the chromatin template. RNA pol II changes its appearance because of the multiple post-translational

modifications (phosphorylation and others) that the carboxyterminal domain (CTD) of the larger subunit (Rpb1) undergoes along the transcription cycle (29). The different phosphorylated forms of CTD make a code that is recognized by specific factors along the different elongation sub-phases (29). The last part of the elongation phase starts with the transcription of a sequence that acts as a signal for the cutting and polyadenylation machinery (30). The most important sequence element for transcriptional termination is the polyadenylation signal (pAS), which, in yeast, consists of three sequence elements: the AU-rich efficiency element (EE), the A-rich positioning element (PE) and the U-rich elements located upstream (UUE) or downstream (DUE) of the cleavage site (30-31). The latter is defined by a pyrimidine followed by multiple adenosines Y(A)n (31). These elements are bound, respectively, by the cleavage factor 1B (CF1B, Hpr1), 1A (CF1A: Clp1, Pcf11, Rna14 & Rna15) and the cleavage and polyadenylation factor (CPF: 13 subunits).. The RNA is then cut , whereupon the coding portion is polyadenylated and the 3' product rapidly degraded (30,46). The elongation complex undergoes a structural modification during these events. Some elongation factors leave the complex shortly before the pAS whereas other remain bound (35). This transition is reflected in the profile of active RNA pol II molecules in the close vicinity before and after the pAS (32).

Xrn1 is a very large (175 kDa, 1528 amino acids in *S. cerevisiae*) protein with pleiotropic function present in all eukaryotes. It was originally cloned a as en enhancer of karyogamy defects (*KEM1*; ref.10) and then isolated again as a DNA-strand transferase (*DST2*; ref 11) together with *DST1* (12), a gene that was shown to encode TFIIS (13). Finally, its name was changed into Xrn1 (eXoRriboNuclease 1) because of its 5'-3' exonuclease activity (14). The structure of the *Klyuveromyces lactis* and *Drosophila* Xrn1 have been determined (15,16). They show that the nucleolytic activity is on its N-terminal part whereas the large C-terminal moiety is not directly involved in nuclease activity. The human orthologue is able to bind G4 tetraplex-containing DNA and RNA substrates (17). It is able to degrade mRNAs that are being translated (18) and the yeast Xrn1-Ribosome complex has been recently published (19). Interestingly, the C-terminal part (downstream Aa 918) is not involved in Ribosome binding. Thus, it is possible that the additional roles of this multifunctional protein rely on the still unassigned parts of its structure.

A fundamental question is how Xrn1-decaysome affects the transcription process. Comparison of the effects of *xrn1Δ*, *ccr4Δ* and other mRNA decay- and tracription-related mutants on *GAL1*, using computational modeling, indicates that Xrn1 and Ccr4 transcriptional functions take place in parallel rather than in a concerted manner (48). For the Ccr4-NOT complex it has been shown that it binds transcription initiation and elongation complexes, and counteracts RNApol II backtracking (7,9). The information available for Xrn1-decaysome is much less abundant. In order to cast light on how Xrn1 contributes to transcription we have performed a series of genome-wide and single-gene experiments using various methods to map the distribution of RNA pol II under Xrn1-perturbed conditions. Our results indicate that the absence of Xrn1 affects transcription during early and late steps of elongation and we suggest that this is an important component of mRNA buffering.

Results

CRAC experiments confirm that lack of Xrn1 decreases transcription rates

Conflicting results on the effect of the *xrn1Δ* mutation on transcription rates have been described, based on different experimental approaches (Fig S1A-B). We have previously shown that genomic run-on (GRO) analyses indicate a global negative effect of *xrn1Δ* on transcription rates across the genome (1). In contrast, results obtained after RNA metabolic labelling (cDTA) with 4-thiouracil (4-tU) were interpreted to support a negative effect of Xrn1 on transcription rates (34).

To solve this apparent contradiction, we adopted a third experimental approach, using RNA pol II CRAC to map the distribution of elongating RNA pol II molecules at nucleotide resolution. For a quantitative analysis of the effect of the *xrn1Δ* mutation we normalized our data to a spike obtained from the addition to each sample of an equal number of *S.pombe* cells expressing a protein modified with the same tag as

yeast RNA Pol II [REF]. Our new analysis confirmed a very significant negative effect of *xrn1Δ* on transcription rates (Fig S1C-E). The similarity between CRAC and GRO data extended to the dependence of the *xrn1Δ* effect on transcription levels. Both in GRO and CRAC experiments, the negative effect caused by the mutation was slightly stronger for highly transcribed genes (Fig S1F-G).

The opposite results obtained by Sun et al (34) using metabolic labelling might be due to not taking into consideration the increased cell volume of *xnr1Δ* cells (discussed in ref. 35) and to a specific effect of 4-tU on *xrn1Δ* cells that provokes increased mRNA stability (Fig S2A). Lack of Xrn1 impedes the 5'-3' mRNA decay pathway. In *xrn1Δ* cells, the alternative 3'-5'pathway, which depends on the exosome, becomes dominant (Fig S2B). Levels of ncRNAS that are degraded by the exosome increased in wild-type cells growing with 4-tU (Fig S2C), suggesting that the 3'-5' mRNA decay pathway might be less efficient in the presence of this compound. As a consequence of this 4-tU-specific impairment of 3'-5' RNA decay, the population of 4-tU-labelled RNAs accumulated in cells lacking Xrn1 during the cDTA labelling time (6 min) might have been artefactually enhanced. One minute is sufficient to complete transcription of the great majority of yeast genes. Then, the increase of 4tU-labelled RNAs observed in the *xrn1Δ* mutant it was likely because labelled RNAs were stabilized, not because transcription rates were higher.

Xrn1 regulates transcription elongation at 5'

In addition to an overall effect on the number of transcribing RNA pol II molecules, lack of Xrn1 produced significantly altered RNA pol II profiles across the genome. Metagene analyses showed an increase in the number of elongating RNA pol II molecules mapped in the wild type shortly downstream of the transcription start site (TSS) and a progressive decline afterwards (Fig S1H). This decline was less pronounced in *xrn1Δ*, which is reflected in the different slopes of the two lines (half of the wild-type slope in *xrn1Δ*) (Fig S1H). The difference in slope was particularly clear in highly transcribed genes and those containing canonical TATA elements, but was also easily detected in other categories of genes, like those encoding ribosomal proteins (Fig 1A, S3A-C and S4A-D).

Different RNA pol II profiles between wt and *xrn1Δ* 5' metagenes were also detected after performing a high-resolution genomic run-on analysis (BioGROseq) (Fig 1B and S5A). Fast depletion of Xrn1, using an AID degron approach (Fig S16A-B), also provoked a change in the CRAC RNA pol II profile of the 5' end metagenes, exhibiting a decrease in the slope after 60 min depletion across the whole genome (Fig S6C) and even before in canonical TATA genes (Fig 1C).

The negative slope of the wild type 5' metagene can be due to an acceleration of elongating RNApol II molecules after the 5' pausing that occurs downstream of the initiation-elongation transition. The less negative slopes in Xrn1-perturbed strains may indicate alteration in elongation rates, as we have already found for *xrn1Δ* in a galactose-controlled long gene (Begley et al, 2019). In order to test this hypothesis we decided to model our Xrn1-degron CRAC data, following an iterative equation approach. As shown in Fig 1D, in both conditions (depleted and non-depleted) estimated elongation rates dropped the same from TSS to position +80. From so on, our model estimated a progressive increase in the elongation rate for the non-depleted condition. In contrast, this acceleration was almost absent in the Xrn1-depleted condition (Fig 1D). These results support an influence of Xrn1 on transcription elongation, as previously proposed (1,36,48).

In the case of Xrn1-depleted data the overall decrease in the number of reads caused by *xrn1Δ* was not detected (compare Fig 1A and C). This is compatible with a scenario where *xrn1Δ* cells exhibit both elongation and initiation defects, the latter being responsible for the general decrease in the number of transcribing RNA pol II molecules. In contrast, Xrn1 depletion by the AID degron system would provoke just the elongation defect, producing no decrease but a slight accumulation of RNA pol II molecules on the gene body, likely as a consequence of its reduced elongation rate. According to this view, the initiation defect detected in *xrn1Δ* might be related, at least partially, to the downregulation of RNA pol II-dependent transcription caused by slow growth (36,48).

RNA pol II CRAC analysis was also performed after depleting the nuclear pool of Xrn1, using an anchor-away approach (Fig S7). After 1 h incubation with rapamycin, we found a slight decrease in the slope of the RNA pol II profile at 5', similar to the one produced by total Xrn1 depletion (compare Fig 1C to 1E, and S1H to S7B). This modest

effect detected might suggest that the functional influence of Xrn1 on transcription elongation depends on its presence in the nucleus. However, we should be very cautious interpreting these results, since we did not found any change in the slope when longer treatments were performed (2 and 5 hours in the presence of rapamycin) and, therefore, we cannot rule out that nuclear Xrn1 depletion was partial and transient.

Lack of Xrn1 produced changes in nucleosome density on gene bodies

We have seen that the change in the slope of CRAC profiles at 5' metagenes produced by the lack of Xrn1 is compatible with a scenario of decreased RNA pol II elongation rate. If this is the case, slower elongation should involve a longer competition for occupancy between elongating RNA pol II molecules and nucleosomes along gene bodies. In order to test this prediction we generated nucleosomal maps of cells lacking Xrn1, using an MNase-seq approach optimized for detecting elongation-related phenomena (37). These maps showed increased occupancy of the two nucleosomes flanking the nucleosome-depleted region (NDR) just upstream the TSS in *xrn1Δ* (Fig 2A). This may be indicative of a lower frequency of PIC assembly, as a consequence of the competition between PIC assembly and nucleosome +1 (38), and is consistent with our hypothesis of overall decrease in transcription initiation in *xrn1Δ*. Alternatively, might be also consistent with less pausing in the early stages of elongation.

In addition, we detected decreased occupancy of nucleosomes in the gene body, downstream of nucleosome +2 (Fig 2A), in a gene length-independent manner (Fig S8A-C). Metagenes obtained after aligning gene groups of different length to the polyadenylation site (pAS) allowed the visualisation of nucleosome occupancy reduction in *xrn1Δ* along the whole gene body (Fig 2B). This is fully consistent with the change in the reduction in elongation rates deduced from the lower slope observed in RNA pol II CRAC profiles after Xrn1 perturbation. Slower elongation would involve higher dwell time for elongating RNA pol II molecules and, as a consequence of it, increased competition with nucleosomes. For instance, after 1h nuclear Xrn1 depletion, the slope decreased during the first 400-500 bp downstream of the TSS, independently of the gene length, and then remained constant until the pAS (Fig S9).

Altogether, the results described above suggest that, in cells lacking Xrn1, nucleosome occupancy of gene bodies decreased due to competition with RNA pol II molecules, which were elongating at a lower rate. This involves a change in the co-transcriptional dynamics of chromatin in *xrn1Δ.* In order to confirm this prediction, we compiled the BioGROseq signals corresponding to every transcribed nucleosome in wild type and *xrn1Δ* cells and represented it after alignment to the dyad axis. We found no differences for +1 nucleosomes, suggesting that dynamics of the first nucleosome (usually occupying the TSS) during transcription initiation was not affected by lack of Xrn1 (Fig 2C). In contrast, we detected significant differences between *xrn1Δ* and the wild type for nucleosomes +2, +3 and +4. Higher density of BioGROseq signal were found before the dyad axis of these nucleosomes in the wild type, reflecting the accumulation of elongating RNA pol II just before the dyad of gene body nucleosomes. In *xrn1Δ* the profiles of actively transcribing RNA pol II molecules across +2, +3 and +4 nucleosomes were wider and shifted to the 3', confirming a different dynamic of elongation immediately downstream of TSS (Fig2C).

Xrn1 perturbation produces prominent pausing of RNA Pol II upstream of the pA site

RNA pol II CRAC also exhibited clear differences between the wild-type and *xrn1Δ* cells at the 3' end. Prominent peaks were found at this region in *xrn1Δ*, usually located shortly upstream of the pA was detected (Fig S10A-C), although internal peaks were also detected, even in antisense orientation (Fig S10B). Metagene analysis confirmed that the presence of this peak in different gene categories (Fig 3A, S3D-F), particularly in highly transcribed genes (Fig S4 E-F). However, with different intensity the vast majority of genes showed higher RNA pol II CRAC values in this region than the wild-type, with a maximal differential signal mapping 40 bp upstream of the pAS (Fig 3B-C).

In contrast, no peak was found in this region in the BioGROseq profiles of *xrn1Δ* (Fig 3D, S5B). Since transcriptional run-on cannot detect backtracked RNA pol II molecules, we consider highly probable that the detected peak represents inactive molecules unable to move forward during very late elongation.

In order to confirm that the reads conforming the detected CRAC peaks corresponded to nascent RNA, all reads that contain a deletion (indicating the presence of a crosslink) were selected and a dataset containing only the position of the deletions

(instead of the whole read) was generated. Genes showing prominent peaks were examined and showed identical patterns to those seen with all the reads (Figure S11).

This accumulation of RNA pol II at the 3' was also detected in metagenes after fast depletion of Xrn1 (Fig S6D, S12A), as it happened in almost every gene (Fig 3E, S10A-C, S12B). We found, also in this case, that the maximal differential CRAC signal mapped 40 bp upstream of the pAS (Fig 3F, S12C). These results strongly indicate a functional influence of Xrn1 in late elongation, that is not due to the slow growth phenotype of *xrn1Δ*. However, we did not detect any RNA pol II CRAC signal accumulation at the 3' end after depleting nuclear Xrn1 with the anchor-away technique, suggesting that this influence of Xrn1 on late elongation might not require its presence in the nucleus (Fig S7C).

Since the inactive RNA pol II peak at the 3' does not seem to be directly related to nuclear Xrn1 but to lack of Xrn1 in the cell, we wondered if other perturbations of mRNA decay might produce similar results. We mapped total RNA pol II in *dhh1Δ* and *ccr4Δ*, two mutants lacking factors involved in decapping and deadenylation during mRNA decay, in a genome wide manner by ChIP seq. Metagenes showed increased levels of RNAPpol II at 3', around the pAS, in the two mutants, similarly to *xrn1Δ* (Fig S13A-C), suggesting that accumulation of RNA pol II at 3' is a response to mRNA decay impairment. In all cases the intensity of RNA pol II accumulation increased with the transcription rate (Fig S13D-F).

Late elongation of regulatory genes with poor nucleosome positioning at 3' is particularly sensitive to lack of Xrn1

Transcription elongation defects can be due to impaired function of the elongation complex or to altered chromatin dynamics in front of elongating RNA pol II. Accumulation of inactive RNA pol II 40 bp upstream of the pAS implies that it takes place in the 3' nucleosome-depleted region that characterizes RNA pol II-dependent genes. Accordingly, no significant alterations of nucleosome maps were detected in *xrn1Δ* cells in that specific position (Fig 2B). We also found no abnormalities in the main histone marks associated to the 5' and 3' chromatin dynamics during transcription. Histone H3 K4-trimethylation, a mark linked with initiation and early elongation, was not significantly changed in *xrn1Δ* in either a highly transcribed gene

(*RPS3*) or a moderately expressed one (*SWD1*) (Fig S14A-B). Similarly, the profile of histone H3 K36-trimethylation, a modification linked to later steps of elongation, did not significantly changed in any of the tested genes (Fig S14C-D).

Since we did not find any significant change of 3' chromatin in *xrn1Δ*, we focused on the elongation complex. Transitions during transcription elongation are linked to modifications of the phosphorylation state of Rpb1 CTD. We analysed it by ChIP in three different genes. Two of them exhibited significant peaks in 3' although with different transcription rates: *RPL40A* (highly transcribed) and *FLC2* (moderately transcribed). A third gene, *RPS3*, was selected for being highly transcribed, although it showed much less accumulation of RNApol II at 3' in *xrn1Δ.* Ser2 phosphorylation is the CTD mark most clearly associated to the elongation step of transcription. We found some alterations in the Ser2 profiles of the three genes tested in *xrn1Δ*, since higher levels of phosphorylation were detected in the mutant in all positions but the TSS (Fig 4A-C). In contrast, lower levels of Tyr1-phosphorylation was found in *FLC2* and in some amplicons of the two other genes tested (Fig 4D-F).

Ser2 and Tyr1 phosphorylation of Rpb1 CTD has been linked to the recruitment of 3' pre-mRNA cleavage factors. We investigated whether lack of Xrn1 involved abnormal recruitment of CF-IA. We found significantly increased binding of Rna15 to amplicons located in the 3' end of these and several other genes (Fig 4G-I and S15A-B). We also found increased levels of Rna14 at the 3' end of *RPS3* (Fig S15C). These results indicate that in Xrn1-deficient cells the RNA pol II elongation complex is altered in two aspects related to 3' mRNA processing: CTD phosphorylation and the binding of CF-IA. This suggests that accumulation of inactive RNA pol II molecules in the 3' end of genes might be the consequence of defective elongation complexes. However, this defect seems to be general and not specific of those genes showing the most prominent peaks.

Since the alterations in the elongation complex did not explain the intensity of 3' peaks we wondered if the chromatin configuration of each gene might do it. We obtained metagene nuclesomal profiles of the 20% top and bottom genes in the distribution of peak intensities shown in Fig 3B. Clear differences were detected in the wild type (Fig 5A). Those genes with the most significant peaks showed a less defined nucleosomal pattern around the polyA site, and a wilder and less-sharp nucleosome depleted region

than bottom genes (Fig 5A). Similar differences between top and bottom genes were detected in *xrn1Δ*, indicating that these differences were neither enhanced nor suppressed by lack of Xrn1 (Fig S16A-B).

We were unable to find any specific DNA motive differentially present in top genes versus bottom ones. However, the nucleotide composition of the pAS region exhibited some differences. Top genes showed a significant enrichment for T nucleotides in the pAS, whereas bottom genes exhibited higher frequency of C nucleotides in the same region (Fig 5C-D). This difference in sequence composition may explain the dissimilar nucleosomal organization of top and bottom genes around the pAS.

These results suggest that those genes with less positioned nucleosomes at their 3' end are more sensitive to the alterations in late elongation caused by lack of Xrn1. In order to explore a possible functional consequence of this scenario we analysed the GO categories enriched in top genes. We found that most of the enriched GO terms were connected to the regulation of biological processes, suggesting that regulatory genes might be particularly sensitive to this phenomenon.

Discussion

We have previously shown that lack of Xrn1 produced downregulation of transcription across the genome (1). In an independent work the group of E. Young also found a positive role for Xrn1 in the transcription of Snf1-dependent genes (44). However, a different study, based on RNA metabolic labelling, described apparently opposite effects of *xrn1Δ* on transcription (34). In this work, using different technical approaches, we demonstrate that Xrn1 perturbation originates significant negative alterations of RNA pol II distribution and, therefore, we confirm that Xrn1 plays a general positive contribution to gene transcription. We also show in this study that Xrn1 perturbation specifically impairs transcription elongation, producing significant changes of elongation rates, after the initiation to elongation transition, and at 3' ends, immediately before pre-mRNA cleavage.

Previous results of Xrn1 were based on the study of mutant cells lacking Xrn1, which exhibit pleiotropic phenotypes, including large cell volume and slow growth, which can indirectly affect transcription (36,45). In this work, we made use of an auxin-degron approach to decrease the risks of indirect effects of *xrn1Δ*.

At the 5' end of gene bodies we observed that Xrn1 perturbations produced a change in the slope of the RNA pol II profiles obtained either with CRAC or BioGROseq. The 50% reduction in slope produced by *xrn1Δ* is in total agreement with the 50% reduction in RNA pol II elongation speed measured by us with the GAL1p-YLR454w system (48). It also fits with the enhanced recruitment of TFIIS across the genome shown by *xrn1Δ*, which indicates higher frequency of backtracking in response to lack of Xrn1 (48).

We also found that nucleosome occupancy was decreased after the +2 position in the gene body, and that the high-resolution distribution of the BioGROseq signal across these nucleosomes was significantly altered in *xrn1Δ*. These results shed light on the contribution of Xrn1 to chromatin transcription from two complementary aspects (nucleosome positioning and RNA pol II activity) and suggest a model were lack of Xrn1 makes the elongation complex unable to keep the wild-type elongation rate, due to different interaction dynamics between RNA pol II and the nucleosome. In this sense, Xrn1 behaves as other elongation factors that modulate RNA pol II pausing through nucleosomes (47).

At the 3' end of gene bodies we observed the accumulation of RNA pol II CRAC signal 40 bp upstream of pAS in Xrn1-deficient cells. This indicates a strong pausing phenomenon. Lack of a similar signal in BioGROseq profiles, based on the run-on capacity of the mapped molecules, suggests that RNA pol II paused at this position become backtracked. This position of the gene body is a key point where the elongation complex undergoes severe changes. Some factors that travel with RNA pol II during elongation leave the complex at this point whereas others remain bound until termination (35). This restructuration is coupled to the 3' processing of pre-mRNA, which is cleaved by CF-IA from the CTD. Arrest of RNA pol II at this point is likely reflecting abnormal dynamics of the elongation complex in this key step. Recruitment of CF-IA to the CTD during elongation is regulated by Tyr1 and Ser2 phosphorylation. We found altered levels of these two CTD phosphorylation marks and enhanced

binding of CF-IA to the elongation complex in Xrn1-perturbed cells. This suggests that the alteration of late elongation that we have detected is due to changes in the elongation complex that, later on, provokes RNA pol II arrest during the elongation/termination transition.

In principle, the two elongation phenotypes that we have described might be caused by a single molecular event derived from Xrn1 perturbation. However, several pieces of information suggest that they are independent. Depletion of the nuclear Xrn1 pool by the anchor-away technique produced the change in the profile slope characteristic of the early elongation phenotype, without causing the accumulation of RNA pol II at the 3'. This suggests that only the first phenomenon is related to a nuclear function of Xrn1. In fact, we detected accumulation of RNA pol II at the 3' in other mRNA decay mutants, like *dhh1Δ* and *ccr4Δ*. In contrast, the general enhancement of TFIIS recruitment shown by Xrn1, likely connected to reduced elongation rates, is not shared by *ccr4Δ* (48).

Although frequent, the peaks of RNApol II shown by *xrn1Δ* at 3' were not equally prominent in all genes. This specificity seems not be related to the alterations of CTD phosphorylation marks or to the increased binding of CF-IA, since these changes also take place in genes with low accumulation of RNApol II at 3'. Our nucleosome maps indicates that these peaks are favored in genes with poor nucleosome positioning at 3'. So it seems that peaks results from the combination of altered elongation complexes in a certain chromatin environment. Intriguingly, genes with significant RNApol II accumulation at 3' are enriched in regulatory functions. This opens an interesting scenario, where genes with regulatory functions may reduce noise by mRNA buffering due to a particularly sensitive response to the mRNA decay/transcription crosstalk.

Methods

Strains.

S. cerevisiae strains used in this study are listed in Table S1. Strains were grown at 30°C, with liquid cultures growing in an orbital shaking incubator at 180 rpm in YP medium (1% yeast extract, 2% peptone) or SC - TRP medium (0.17% yeast nitrogen bases (YNB), 0.5% ammonium sulphate and amino acids leucine, histidine, lysine and nitrogenous bases adenine and uracil) and containing either 2% glucose (YPD) or 2% galactose (YPGal) as a carbon source.

For transcriptional shut-off assays, cells were grown in YPGal until reaching an OD_{600nm} of 0.2-0.3. At this point, 4mM of 4-thiouracil (Sigma) or DMSO was added to the media and left to grow for an additional 2 hours until reaching OD_{600nm} of approximately 0.5. Then, a sample was taken, and immediately after, glucose 4% was added to the culture. Samples were taken at the indicated times after glucose addition.

For obtaining CRAC samples, strains were grown in SC –TRP until an OD_{600nm} of 0.5-0.6. In parallel *Schizosaccharomyces pombe* was also grown to an OD_{600nm} of 0.5-0.6 in minimal media (EMM 0.5X), in order to add 1% to the culture before cross-linking as a spike-in. To the XRN1-AID strain 0.2mM of auxin (3-Indoleacetic acid; Sigma-Aldrich) was added to the media 30 and 60 minutes before harvesting. To the XRN1-AA strain 1 µg/ml of rapamycin (Sigma) was added to the media 60 minutes before harvesting.

RNA extraction and RT-qPCR.

Cells were grown to log phase and 10 ml was harvested by centrifuging for 2 minutes at 4000 rpm and flash freezing the cells in liquid nitrogen. Total RNA was purified using hot phenol–chloroform method as described previously (Amberg et al., 2005) and reverse-transcribed to cDNA using M-MLV Reverse Transcriptase (Promega). A relative real-time quantitative PCR was then carried out for all the genes studied (Table S2) against *SCR1* using SYBR Green Premix Ex Taq (Takara) in a Light Cycler 480 II (Roche).

To determine the mRNA half-lives, we used a transcription shut-off assay, collecting samples at 5, 10, 20, 30, 40, 50 and 60 minutes after glucose addition. mRNA levels were then determined with RT-qPCR and half-lives were estimated by calculating the time it takes for half of the initial amount of RNA to be degraded. Primers used are listed in Table S2.

Chromatin immunoprecipitation (ChIP).

Yeast strains were grown to exponential phase and 50 ml were taken for each sample. The ChIP experiments were performed as previously described (Rodríguez-Gil et al., 2010), except that anti-Rpb3 (ab81859; Abcam), anti-Ser2P (ab5095; Abcam), Anti-Ser5P (ab5131; Abcam), Anti-Ser7P (4E12; Chromotek), anti-Tyr1P (3D12; Merck), anti-Thr4P (1G7; Merck), anti-H3K4me3 (ab8580; Abcam) or anti-H3K36me3 (ab9050; Abcam) antibodies and Sheep anti-Mouse IgG Dynabeads (Invitrogen) were used. Genes were analysed by quantitative real-time PCR in triplicate using primers listed in Table S2.

CRAC.

Cells grown until exponential phase were crosslinked at UV 254nm with a Megatron for 50s and harvested by centrifugation. The cells were then resuspended in TN150 buffer (50mM Tris pH 7.8, 150mM NaCl, 0.1% NP-40 and 5mM β-mercaptoethanol) supplemented with protease inhibitors (complete, Mini, EDTA-free Protease Inhibitor Cocktail). This suspension was flash frozen in droplets and cells were mechanically broken using the Mixer Mill MM 400. The resulting cell "powder" was thawed and treated for one hour at 25 °C with DNase I (165 U/g of cells). The cells were centrifuged and subsequent purifications steps were performed essentially as described (Granneman et al., 2009) with minor modifications. The adaptors were modified in order to sequence RNA molecules from the 3'-end. The RNA was recovered after proteinase K treatment by phenol-chloroform extraction and reverse transcribed using specific primers. The resulting cDNA was amplified with multiple PCR reactions in a final volume of 25 µl using the following conditions: 0.4 µM of each primer, 0.2mM dNTP, 2.5 U LA Taq DNA polymerase from Takara, 1x LA PCR Buffer II and 2 µl of complementary DNA per reaction with the programme: 2' at 95 °C, (30'' at 95 °C, 45'' at 58 °C, 1' at 72 °C) × 13 cycles, 5' at 72 °C. All the PCR reactions were pooled together and treated with 200 U of Exonuclease I (NEB) per ml of PCR reaction for 1 h at 37 °C. After Exonuclease I inactivation for 20' at 80 °C, DNA was purified with PCR clean up columns (NucleoSpin Gel and PCR Clean-up, Macherey-Nagel) and sequenced using Illumina technology.

BioGRO-seq

The Bio-GRO protocol was essentially as described in (Jordán-Pla et al., 2016) for tiling array analysis, but modified for high-throughput sequencing. Detailed description will be published elsewhere.

MNase

The MNase digestion was performed as described in (37). Briefly, 500 ml of exponentially grown yeast culture was cross-linked with formaldehyde. Cells were washed and resuspended in Buffer Z2. Zymolyase was added and cells were incubated for 30 min at 30 °C to obtain spheroplasts. Spheroplasts were incubated with different amounts of micrococcal nuclease (from 500 to 10 mU). Protein was degraded by Proteinase K and DNA was obtained by phenol-chloroform-isoamyl extraction and ethanol precipitation. Digested DNA was resolved on an agarose gel and the band corresponding to mononucleosomes was purified and sent for Ilumina sequencing. Naked DNA was obtained as before but MNase was added after DNA extraction instead of before, and a band with similar digestion as the mononucleosomes was purified and sent for sequencing.

Bioinformatics

CRAC samples were demultiplexed using the pyBarcodeFilter script from the pyCRAC utility suite. Subsequently, the 3' adaptor is clipped with Cutadapt and the resulting insert is quality trimmed from the 3'-end using Trimmomatic rolling mean clipping (window size =5, minimum quality =25). At this stage, the pyCRAC script pyFastqDuplicateRemover is used to collapse PCR duplicates and ensure each insert is represented only once. Each unique insert in our library is associated with a six nucleotides random tag within the 5' adaptor. The resulting sequences are reverse complemented with Fastx_reverse_- complement (part of the fastx toolkit), and mapped to the R64 genome (sgd) with bowtie2 (-N 1 –f). Read counts were normalized relative to reads derived from an *S. pombe* spike-in. The *S. pombe* spike cells contain a non-relevant protein tagged with the same HTP tag that was co-purified with the *S. cerevisiae* sample. We then performed a metagene analysis using a package available

for Python, ngsplot. We obtained the scatterplots, boxplots and density plots by counting the number of reads within the ORF of a gene using HTSeq, and then plotting this data in R.

The paired-end sequencing data obtained from MNase was aligned to the *S. cerevisiae* reference genome (SacCer2) with the GEM software (Marco-Sola et al., 2012). The resulting BED files of all samples were run through the DANPOS v2.1.2 (Chen et al., 2013) algorithm, in which reads were clonally cut to remove any potential PCR amplification bias, smoothed and adjusted for nucleosome size. DANPOS pools the replica of the same condition and can use naked data as a background correction. Metagene spectral analysis periodograms were calculated with PAST, v3 (Hammer et al., 2001).

Estimation of elongation rates

To estimate the RNA polymerase elongation rates along the genomic region, we divide the region into spatial bins $i \in \{0,1,2,\dots\}$ where $i = 0$ corresponds to the Transcription Start Site (TSS). The RNA polymerase hops from bin i to $i+1$ with rate k_i that can be interpreted as the elongation rate at that genomic region. Let k_{TSS} be the arrival rate of RNA polymerase to the TSS, then one can write the following iterative equations based on the same inflow and outflow of polymerases at each location

$$k_{TSS}\,(1 - R_0) = k_0\,R_0\,(1 - R_1)$$

$$k_0\,R_0\,(1 - R_1) = k_1\,R_1(1 - R_2)$$

$$k_i\,R_i\,(1 - R_{i+1}) = k_{i+1}\,R_{i+1}(1 - R_{i+2})$$

where $i \in \{0,1,2,\dots\}$, and R_i denotes the probability of RNA polymerase occurrence in the spatial bin i. To estimate R_i from the mean number of reads we divide it by a sufficiently large constant that is chosen such that $R_0 \ll 1$. Given the estimates of R_i we solve the above equations iteratively to find k_i normalized by k_{TSS} .

Western blot

Laemmli-boiled crude extracts were run on a SDS-polyacrylamide gel and transferred to nylon membranes (Hybond-ECL). After blocking with Tris-buffered saline containing 0.1% Tween 20 and 5% milk, the following primary antibodies were used: anti-FLAG M2 (Sigma-Aldrich), anti-GFP (Roche) and anti-L1. Finally, the membrane was incubated with peroxidase-conjugated goat anti-mouse IgG and proteins were detected using a chemiluminescence detection kit (Super-Signal West Pico, Pierce) and a ChemiDoc™ MP system (Bio-Rad).

Sucrose gradient centrifugation

For polysome preparations 200 ml cultures were grown in YPD and harvested at an OD_{600nm} between 0.5 and 1. Cycloheximide was added to a final concentration of 0.1 mg/ml before harvesting for 10 minutes. Cell extracts were obtained by adding lysis buffer (10 mM Tris-HCl (pH 7.5), 100 mM NaCl, 30 mM and 0.2 mg/ml of heparin) and glass beads, and vortexing for 8 minutes at 4 °C. The supernatant was recovered after centrifugation and flash frozen. Thawed extracts (10 absorption units at 260 nm) were layered onto 11.2 ml of 7 to 50% linear sucrose gradients that were prepared in 50 mM Tris-acetate (pH 7.5), 50 mM NH4Cl, 12 mM MgCl2, 1 mM dithiothreitol. The gradients were centrifuged at 39,000 rpm in a Beckman SW41 rotor at 4°C for 2 h 45 min. Gradient analysis was performed with an ISCO UV-6 gradient collector and continuously monitored at 254 nm. Fractions were collected every 30 s for 9 min (18 in total).

For western analysis, proteins (0.5 ml of each fraction) were precipitated by addition of trichloroacetic acid to a final concentration of 10%, followed by incubation on ice for 10 min. Proteins were pelleted by centrifugation for 10 min at 4 °C. Pellets were washed twice with 1 ml of ice-cold acetone and finally resuspended in 20 µl of 2X laemmli buffer. Every two fractions were mixed together and aliquots of 20 µl were loaded onto 10% SDS-polyacrylamide gels and analyzed by western blot analysis.

Acknowledgements

We thank M.E. Pérez-Martínez and M. Barneo-Muñoz for the BioGROseq setup.

Funding:

This work has been supported by grants from the Spanish Ministry of Economy and Competitiveness, and European Union funds (FEDER) [BFU2016-77728-C3-1-P to S. C.], [BFU2016-77728-C3-3-P and BFU2015-71978-REDT to J.E.P-O & P.E.], [BFU2016-77728-C3-2-P to F.N.]; by FPI grants from the Spanish Government to V.B and A.C-B; by the Regional Andalusian Government [P12-BIO1938MO and BIO271 to S. C.], [BIO258 to F.N.] and from the Regional Valencian Government [PROMETEO II 2015/006 to J.E.P-O]. Funding for open access charge: [BFU2016-77728-C3-1-P].

References

1. Haimovich, G et al. 2013. Cell 153, 1000-1011

2. Choder M. 2011. Cell Logist. 1:37-40

3. Miller JE, Reese JC 2012. Crit Rev Biochem Mol Biol. 47:315-333

4. Schmid, M. and Jensen, T.H. 2018. Nat. Rev. Genet. 19:519-529

5. Rambout X et al. 2016 Nat Struct Mol Biol. 23:663-672

6. Abernathy et al., 2015, Cell Host & Microbe 18, 243–253

7. Gupta,I., Villanyi,Z., Kassem,S., Hughes,C., Panasenko,O.O., Steinmetz,L.M. and Collart,M.A. (2016) Translational Capacity of a Cell Is Determined during Transcription Elongation via the Ccr4-Not Complex. Cell Rep., 15, 1782–1794.

8. Bernat-Blasco et al. (2019). Nat. Commun. 10(1):1298

9. Collart,M.A. (2016) The Ccr4-Not complex is a key regulator of eukaryotic gene expression. Wiley Interdiscip. Rev. RNA, 7, 438–454.

10. Kim J, et al. (1990) kem mutations affect nuclear fusion in Saccharomyces cerevisiae. Genetics 126(4):799-812.

11. Dykstra, CC et al. (1991) Cloning and characterization of DST2, the gene for DNA strand transfer protein beta from Saccharomyces cerevisiae. Mol Cell Biol 11(5): 2583–2592.

12. Clark AB, et al. (1991) Isolation, DNA sequence, and regulation of a Saccharomyces cerevisiae gene that encodes DNA strand transfer protein alpha. Mol Cell Biol 11(5):2576-82.

13. Davies CJ, et al. (1990) Homologue of TFIIS in yeast. Nature 345(6273):298

14. Larimer FW and Stevens A (1990) Disruption of the gene XRN1, coding for a 5'----3' exoribonuclease, restricts yeast cell growth. Gene 95(1):85-90.

15. Chang, JH et al (2011). Nat Struct Mol Biol. 18(3): 270–276.

16. Jinek, M. (2011). Mol Cell. 41(5):600-8.

17. Bashkirov, V. I., Scherthan, H., Solinger, J. A., Buerstedde, J. M., and Heyer, W. D. (1997). A mouse cytoplasmic exoribonuclease (mXRN1p) with preference for G4 tetraplex substrates. J. Cell Biol. 136, 761–773

18. Pelechano, V. et al (2017). Cell.

19. Tesina, P et al. (2019) Nature Structural & Molecular Biology 26, 275–280

20. Jayasha Shandilya, Stefan G.E. Roberts. 2012. The transcription cycle in eukaryotes: From productive initiation to RNA polymerase II recycling. Biochimica et Biophysica Acta (BBA) - Gene Regulatory Mechanisms, 1819: 391-400

21. Huisinga, K. L. & Pugh, B. F. (2004) A genome-wide housekeeping role for TFIID and a highly regulated stress-related role for SAGA in Saccharomyces cerevisiae. Molecular cell 13, 573- 585.

22. Basehoar, A. D., Zanton, S. J. & Pugh, B. F. Identification and distinct regulation of yeast TATA box-containing genes. Cell 116, 699-709 (2004).

23. Paper chromatin organization in RP genes

24. Pelechano et al (2009) PLoS Genet.

25. García-Molinero V et al (2018). Epigenetics Chromatin. 2018 Mar 29;11(1):13

26. Rodríguez-Navarro S. Insights into SAGA function during gene expression. EMBO Rep. 2009;10:843–50

27. Mason PB, Struhl K 2005. Distinction and relationship between elongation rate and processivity of RNA polymerase II in vivo, Mol. Cell 17: 831- 840.

28. Gómez-Herreros et al (2012). Nucleic Acids Res. 40(14):6508-19.

29. Buratowski S. Progression through the RNA polymerase II CTD cycle. Mol Cell 2009; 36:541-546

30. Millevoi S, Vagner S 2010. Molecular mechanisms of eukaryotic pre-mRNA 3′ end processing regulation. Nucleic Acids Res 38: 2757–2774.

31. van Helden J, del Olmo M, Pérez-Ortín JE 2000 Statistical analysis of yeast genomic downstream sequences reveals putative polyadenylation signals.Nucleic Acids Res. 8(4):1000-10.

32. Jordan-Pla et al. (2015). Nucleic Acids Res. 2015 Jan;43(2):787-802.

33. Tuck, AC & Tollervey D 2013. A Transcriptome-wide Atlas of RNP Composition Reveals Diverse Classes of mRNAs and lncRNAs Cell. 154(5): 996–1009.

34. Sun,M., Schwalb,B., Pirkl,N., Maier,K., Schenk,A., Failmezger,H., Tresch,A. and Cramer,P. (2013). Global analysis of Eukaryotic mRNA degradation reveals Xrn1-dependent buffering of transcript levels. Mol. Cell, 52, 52–62.

35. Mayer A, Lidschreiber M, Siebert M, Leike K, Söding J, Cramer P. 2010. Uniform transitions of the general RNA polymerase II transcription complex. Nat Struct Mol Biol. 17:1272-8.

36. García-Martínez J, Troulé K, Chávez S, Pérez-Ortín JE. 2016. Growth rate controls mRNA turnover in steady and non-steady states. RNA Biol. 13:1175-1181.

37. Gutiérrez G, Millán-Zambrano G, Medina DA, Jordán-Pla A, Pérez-Ortín JE, Peñate X, Chávez S. 2017. Subtracting the sequence bias from partially digested MNase-seq data reveals a general contribution of TFIIS to nucleosome positioning. Epigenetics Chromatin 10:58.

38. Rhee HS, Pugh BF. 2012. Genome-wide structure and organization of eukaryotic pre-initiation complexes. Nature. 483:295-301.

39. Kruk JA, Dutta A, Fu J, Gilmour DS, Reese JC. 2011. The multifunctional Ccr4-Not complex directly promotes transcription elongation. Genes Dev. 25:581-93.

40. Dronamraju R, Hepperla AJ, Shibata Y, Adams AT, Magnuson T, Davis IJ, Strahl BD. 2018. Spt6 Association with RNA Polymerase II Directs mRNA Turnover During Transcription. Mol Cell. 70:1054-1066.

41. Bentley DL. 2014. Coupling mRNA processing with transcription in time and space. Nat Rev Genet. 2014. 15:163-75.

42. Petty E, Pillus L. Balancing chromatin remodeling and histone modifications in transcription. 2013. Trends Genet. 29:621-9.

43. Singh P, James RS, Mee CJ, Morozov IY. (2019). mRNA levels are buffered upon knockdown of RNA decay and translation factors via adjustment of transcription rates in human HepG2 cells. RNA Biol. doi: 10.1080/15476286.2019.1621121. [Epub ahead of print].

44. Braun KA, Young ET. 2014. Coupling mRNA synthesis and decay. Mol Cell Biol 34:4078–4087. doi:10.1128/MCB.00535-14.

45. Mena A, Medina DA, García-Martínez J, Begley V, Singh A, Chávez S, Muñoz-Centeno MC, Pérez-Ortín JE. 2017. Asymmetric cell division requires specific mechanisms for adjusting global transcription. Nucleic Acids Res. Dec 1;45(21):12401-12412.

46. Porrua O, Boudvillain M, Libri D. 2016. Transcription Termination: Variations on Common Themes. Trends Genet. 32(8):508-522. doi: 10.1016/j.tig.2016.05.007.

47. Ehara H, Kujirai T, Fujino Y, Shirouzu M, Kurumizaka H, Sekine SI. 2019. Structural insight into nucleosome transcription by RNA polymerase II with elongation factors. Science. 363:744-747.

48. Begley V, Corzo D, Jordán-Pla A, Cuevas-Bermúdez A, Miguel-Jiménez L, Pérez-Aguado D, Machuca-Ostos M, Navarro F, Chávez MJ, Pérez-Ortín JE, Chávez S. 2019. The mRNA degradation factor Xrn1 regulates transcription elongation in parallel to Ccr4. Nucleic Acids Res. 47:9524-9541.

Figure legends

Figure 1. Xrn1 perturbation alters RNA pol II profiles downstream of the TSS. A) A metagene plot of the CRAC data for all TATA genes aligned by their transcription start site (TSS) shows that there is a global reduction in RNA bound to total RNA pol II and a decrease in the slope in a *xrn1Δ* strain (in orange) compared to the wt (in green). B) A similar metagen plot of BioGRO-seq data for all TATA genes shows the same effect as in A for the nascent mRNA produced by active RNA pol II. C) The fast depletion of Xrn1 using the auxin-degron system shows a progressive change in the slope of the CRAC data of all TATA genes but with a small increase in the global number of reads. D) Estimation of elongation rates from the CRAC data after fast depletion shown in C, after solving iterative equations based on the same inflow and outflow of polymerases at each location (see Methods). E) The fast depletion of Xrn1 from the nucleus using the anchor-away protocol also shows a change in the slope compared to the wt (green).

Figure 2. Lack of Xrn1 changes the chromatin landscape and the distribution of active RNA pol II molecules through nucleosomes. A) Metagene analysis of the MNase-seq data shows increased occupancy of the nucleosomes flanking the TSS and decreased occupancy of nucleosomes in the gene body in a *xrn1Δ* strain (in blue) compared to the wt (orange). The red arrow indicates where the profile changes from higher nucleosome occupancy to lower occupancy in *xrn1Δ*. B) The same analysis as in A but around the polyA site (pAS) and dividing the genes depending on the gene length into 3 groups according to gene length. The red arrows indicate the intersection between wt and *xrn1Δ* profiles. C) Compiled BioGRO-seq signals for the wt and *xrn1Δ* in +1, +2, +3 and +4 nucleosomes aligned to the dyad axis. Profiles of active RNA pol II were unchanged in the +1 nucleosome but were wider and shifted to the 3' in *xrn1Δ* in the subsequent nucleosomes (+2, +3 and +4).

Figure 3. Xrn1 perturbation produces an alteration of total RNA pol II profiles at the 3' end of genes. A) Metagene analysis of RNA pol II-CRAC profiles in *xrn1Δ* (orange) compared to the wt (green) around the polyA site (pAS) of TATA-containing genes. B)

Heatmap of the *xrn1Δ/*wt ratio of CRAC data, showing a widespread increase in the number of *xrn1Δ* reads just before the pAS (in red). Genes are ordered regarding the peak intensity. C) Metagene representing the mean of all genes shown in the previous heatmap. D) Metagene plot of the BioGRO-seq data in wt and *xrn1Δ* cells, showing that there is no accumulation of active RNA pol II in *xrn1Δ* at the 3' end of TATA-containing genes. E) Heat map of ratios, as in B, but 30 minutes after Xrn1 depletion (auxin-degron CRAC-seq data) divided by data before depletion. F) Metagene representing the mean of all genes shown in the previous heatmap.

Figure 4. Lack of Xrn1 alters Ser2 and Tyr1 phosphorylation of RNApol II CTD and enhances the binding of CF-IA. Anti-phosphorylated Ser2-CTD ChIP experiment show slightly increased levels of this CTD modification in *xrn1Δ* strain in three genes: *FLC2* (A), *RPL40A* (B) and *RPS3* (C). We represent IP signal normalized by Rpb3 ChIP, made on the same extracts in parallel. D-F) Anti-phosphorylated Tyr1-CTD ChIP, normalized by Rpb3 ChIP, for the same genes. Slight decrease in Tyr1 phosphorylation was detected. G-I) Anti-Rna15-TAP ChIP, normalized by Rpb3 ChIP, shows increased binding of Rna15 to 3' in *xrn1Δ* cells. In all cases the mean and standard deviation of three biological replicates is shown. All ChIP experiments were performed using the TAP-tagged Rna15 strain. * stands for a statistically significant difference between wt and mutant (Student's t-test with $p<0.05$).

Figure 5. Genes with poor nucleosome positioning at 3' are more sensitive to RNApol II arrest in *xrn1Δ*. A) Nucleosomal maps of the pAS regions of genes showing different intensity of RNApol II peaks at 3' in *xrn1Δ*, obtained by resistance to micrococcal nuclease. Metagenes were calculated for two sets of genes from the distribution shown in Fig 3C: genes ranking in the 20% top (top) and 20% bottom (bottom). B) Frequency of C and T in the nucleotide composition of top and bottom genes. 10 nucleotide moving average is shown. C) Significance of the difference in C and T nucleotide composition between top and bottom genes, calculated by a Chi square test. D) Functional GO categories enriched in top genes.

Supplementary Tables

Table S1. Yeast strains used in this study.

Yeast strain	***Relevant genotype***	***Reference***
RPB1-HTP	*W303 RPB1-HTP::TRP*	D. Libri Lab
VBY70	*W303 RPB1-HTP::TRP Xrn1::KanMx4*	This work
VBY67	*W303 XRN1-FRB-GFP::kanMx4 RPBL13-2xFKBP12::TRP tor1-1 frp1::LEU RPB1-HTP::URA*	This work
VBY72	*W303 XRN1-AID-FLAG::KanMx4-TIR1 RPB1-HTP::TRP*	This work
Xrn1-AID	*BY4741 XRN1-AID-FLAG::KanMx4-TIR1*	D. Libri Lab
wt	*BY4741*	Euroscarf
xrn1Δ	*BY4741 Xrn1::KanMx4*	Euroscarf
ccr4Δ	*BY4741 Ccr4::KanMx4*	Euroscarf
VBY129	*BY4741 Xrn1::KanMX4 Ccr4::KanMx4*	This work
VBY83	*BY4741 Rna15-TAP::His*	Euroscarf
VBY90	*BY4741 Rna15-TAP::His Xrn1:.KanMx4*	This work
VBY82	*BY4741 Rna14-TAP::His*	Euroscarf
VBY86	*BY4741 Rna14-TAP::His Xrn1::KanMx4*	This work

Table S2. Primers used in this work.

Primer	**Sequence 5'-3'**	**Use**

L3-6N-GAG	/5rApp/GCTctcNNNNNNAGATCGGAAGAGCGTCGTGTAGGGAAAGAGTGT/3ddC/	3' adapter (CRAC)
L3-6N-UGC	GCTgcaNNNNNNAGATCGGAAGAGCGTCGTGTAGGGAAAGAGTGT	3' adapter (CRAC)
L3-6N-ACU	GCTagtNNNNNNAGATCGGAAGAGCGTCGTGTAGGGAAAGAGTGT	3' adapter (CRAC)
L3-6N-CUA	GCTtagNNNNNNAGATCGGAAGAGCGTCGTGTAGGGAAAGAGTGT	3' adapter (CRAC)
L5miRCat	/5InvddT/CTTGrGrCrArCrCrCrGrArGrArArUrUrCrCrA	5' adapter (CRAC)
RT L3-2	ACACTCTTTCCCTACACGACGCTCTTCCG	RT (CRAC)
P5_3prime	AATGATACGGCGACCACCGAGATCTACACTCTTTCCCTACACGACGCTCTTCCGATCT	PCR (CRAC)
miRCat_PCR2	CAAGCAGAAGACGGCATACGAgatcCTTGGCACCCGAGAAT	PCR (CRAC)
GAL7_555-654_up	TGGTGCTTAGAATCCATCCCTAG	RT-qPCR
GAL7_555-654_low	GACGTAATCGGCAAACAAATCAGT	RT-qPCR
GAL1-1040F	AAGAGTCTCTCGCCAATAAGAAAC	RT-qPCR
GAL1-1142R	GATGTTGTTAAGTAGTCTCTTGTG	RT-qPCR
GAL10_915-1015_up	CAAAGTTACGGGCAGAAGAGC	RT-qPCR
GAL10_915-1015_low	CTTCAACCTGCAACTCGGTCT	RT-qPCR
3800-4100-191F (*YLR454w*)	GATATGCTTCAATCCGACAGAGAG	RT-qPCR
3800-4100-258R (*YLR454w*)	TCAACAGTTACCGATGGTATTAAAGG	RT-qPCR
SCR1_RTup	GTCTCTCTGTCTGGTGCGGC	RT-qPCR

SCR1_RTlow	CACGGGTCACCTTTGCTGA	RT-qPCR
NEL025c F (474)	GCAAAGATCTGTATGAAAGG	RT-qPCR
NEL025c R (475)	CGCAGAGTTCTTACCAAACG	RT-qPCR
Snr13 F (1117)	GAGTGCATTTGGCTCGAGTTGC	RT-qPCR
Snr13 R (1118)	TTCCACACCGTTACTGATTT	RT-qPCR
ACT1 F (337)	ATGTTCCCAGGTATTGCCGA	RT-qPCR
ACT1 R (378)	ACACTTGTGGTGAACGATAG	RT-qPCR
XUT1092 F	TTCAACGTGAAATTGGTGGA	RT-qPCR (Wery et al., 2016)
XUT1092R	AGTGACATCTGGCGCTGATA	RT-qPCR (Wery et al., 2016)
XUT1186 F	TCCAGTGATGTGGACGAGAA	RT-qPCR (Wery et al., 2016)
XUT1186 R	AAGCCGTTATGAAGACTCCAA	RT-qPCR (Wery et al., 2016)
SCR1 F	GGCTGTAATGGCTTTCTGG	RT-qPCR (Wery et al., 2016)
SCR1 R	ATCCCGGCCGCCTCCATCAC	RT-qPCR (Wery et al., 2016)
rps3-12-983F	AGCAAACAAACTACAAAAATG	ChIP qPCR
rps3-12-1099R	ACCTTCTTCAGCTAATTCTCTG	ChIP qPCR
rps3-13-1039F	TGACGGTGTCTTCTACGCTGA	ChIP qPCR
rps3-13-1142R	CTTCGGTCTTGGTTGGAGTGA	ChIP qPCR
rps3-14-1121F	GTCACTCCAACCAAGACCGAA	ChIP qPCR
rps3-14-1221R	TGAACCAACAAAGTTAATTCG	ChIP qPCR
rps3-15-1198F	CAACGAATTAACTTTGTTGGTT	ChIP qPCR
rps3-15-1302R	TGAGCGACAGCGGACAAAC	ChIP qPCR
rps3-16-1285F	TTTGTCCGCTGTCGCTCA	ChIP qPCR

rps3-16-1385R	ATTCCATAACGTATCTGACGA	ChIP qPCR
rps3-17-1381F	GGAATCTGGTGCTAAGGGTTG	ChIP qPCR
rps3-17-1481R	CAGAGTGAATCAAGAAACCGT	ChIP qPCR
rps3-18-1483F	TCAACCAGTCAACGACTTCAT	ChIP qPCR
rps3-18-1587R	CTGCTCTTAGCTGGGTCTCTC	ChIP qPCR
rps3-19-1566F	TGAGAGACCCAGCTAAGAGCA	ChIP qPCR
rps3-19-1666R	GACAGATGGAGCAAGAATTGG	ChIP qPCR
rps3-20-1653F	TTGCTCCATCTGTCAAGGACT	ChIP qPCR
rps3-20-1786R	ACGGCAATATGCAAGAAACCG	ChIP qPCR
RPS3-1776-F	CTAGTGCACTTAATTGTTGCGG	ChIP qPCR
RPS3-1863-R	ACAACTAGTTTCAACGCACTGC	ChIP qPCR
RPS3-1842-F	GCAGTGCGTTGAAACTAGTTG	ChIP qPCR
RPS3-1970-R	CCTGTAAGCTGAGAAAGATGAAC	ChIP qPCR
RPS3-1967-F	CAGGACGATTTCTCGGATATG	ChIP qPCR
RPS3-2089-R	TAAAAGAGCAAAAAAGAGCGC	ChIP qPCR
ADH1 1 up	GCACGGTGACTGGCCATT	ChIP qPCR
ADH1 1 low	TCTTCCAGCCCTTAACGTTTTC	ChIP qPCR
ADH1 2 up	TGCTAACTTGATGGCCGGTC	ChIP qPCR
ADH1 2 low	AGACTCTGTAACCCATAGCCTTGG	ChIP qPCR
ADH1 3 up	ACGTCGGTAACAGAGCTGACAC	ChIP qPCR
ADH1 3 low	TTCTGGCAAGGTAGACAAGCC	ChIP qPCR
ADH1_+988_F	GTCAAATCGTTGGTAGATACG	ChIP qPCR
ADH1_+1103_R	CTAAGAGTCACTTTAAAATTTGTATACAC	ChIP qPCR
ADH1_+1119_F	AAGTGACTCTTAGGTTTTAAAACG	ChIP qPCR

ADH1_+1215_R	CGGTAGAGGTGTGGTCAATA	ChIP qPCR
SWD1_2_F	GTATGTACACATTTCTGCTGATGTG	ChIP qPCR
SWD1_2_R	GGGGAAGATCCAATATAATCGTCAACC	ChIP qPCR
SWD1_4_F	GAACATCCTGAGAAGCTCACACATAC	ChIP qPCR
SWD1_4_R	CGTAAATAACAAGTGCTCCATTGGC	ChIP qPCR
SWD1_7_F	CAATGGCTGGATGCTAAAAGGC	ChIP qPCR
SWD1_7_R	CGTCTGATTTACTGAGAAGGCTTGC	ChIP qPCR
SWD1_9_F	GTTGGAACTTCAAAAGGTTGGCTAG	ChIP qPCR
SWD1_9_R	GCTAATCTTTCACCATTTTGCGAGA	ChIP qPCR
SWD1_11_F	GTTGACCTTAGAGCATAAGTACCAGG	ChIP qPCR
SWD1_11_R	CAGAAGAACCATGTGTAGAAGCGAC	ChIP qPCR
SWD1_14_F	CTGTTGTTATTCCGCCAAAGTGG	ChIP qPCR
SWD1_14_R	CTTGCTGCTGTTCTGCCTCATC	ChIP qPCR
SWD1_16_F	CGGTTCACAATCCCTACAGATTATACG	ChIP qPCR
SWD1_16_R	CTATACCTCTTCAGTGTCAGTTGCC	ChIP qPCR
RPL5 1 up	CTATACCTCTTCAGTGTCAGTTGCC	ChIP qPCR
RPL5 1 low	CTTGGCCTTGTGTTGGGTG	ChIP qPCR
RPL5 2 up	TGGGTTTGGACGAAACTTACAA	ChIP qPCR
RPL5 2 low	AGAGCACCGAAAACTCTGGC	ChIP qPCR
RPL5 3 up	CACTTCTGCTCACGAAGCTATCA	ChIP qPCR
RPL5 3 low	GATCTTGGCAGCAACACGAG	ChIP qPCR
RPL25 1 up	CACGAGAAAATTGAGAGGAAGATAGA	ChIP qPCR
RPL25 1 low	CGTGTGGTTTTCGTATCTCATCA	ChIP qPCR
RPL25 2 up	AGCAACGTAATTATCGGGCTCA	ChIP qPCR

RPL25 2 low	AACTTCCACAGCATCAACGCT	ChIP qPCR
RPL25 3 up	TGGTTTTCCAAGTTTCCATGAA	ChIP qPCR
RPL25 3 low	AACTTCGTATAATTCCTTGACGGC	ChIP qPCR
RPS3 1 up	TTTTTGAACATTGTTTTGATAACTGAAA	ChIP qPCR
RPS3 1 low	AGAGATTAAAGCGACCATTTTTGTAGT	ChIP qPCR
RPS3 2 up	AAGAGATTCAAGTACGCTCCAGGT	ChIP qPCR
RPS3 2 low	GCGGACAAACCACGGTCT	ChIP qPCR
RPS3 3 up	GGTTGTGAAGTTGTTGTTTCCG	ChIP qPCR
RPS3 3 low	AAACCGTCAGCAAATTTCATAGC	ChIP qPCR
RPS8 1 up	CGTCACAAAAGATCCGCTACC	ChIP qPCR
RPS8 1 low	TCTTGGTGTTGGCTGGTTGA	ChIP qPCR
RPS8 2 up	CCAAGAAGACCAGAATTGCTGG	ChIP qPCR
RPS8 2 low	AGCATCAATTTGGACAATGGC	ChIP qPCR
RPS8 3 up	GCTGCTTCTGCCAAGATCG	ChIP qPCR
RPS8 3 low	CGGATTGACCTGGTCTGGAA	ChIP qPCR

Figure 1

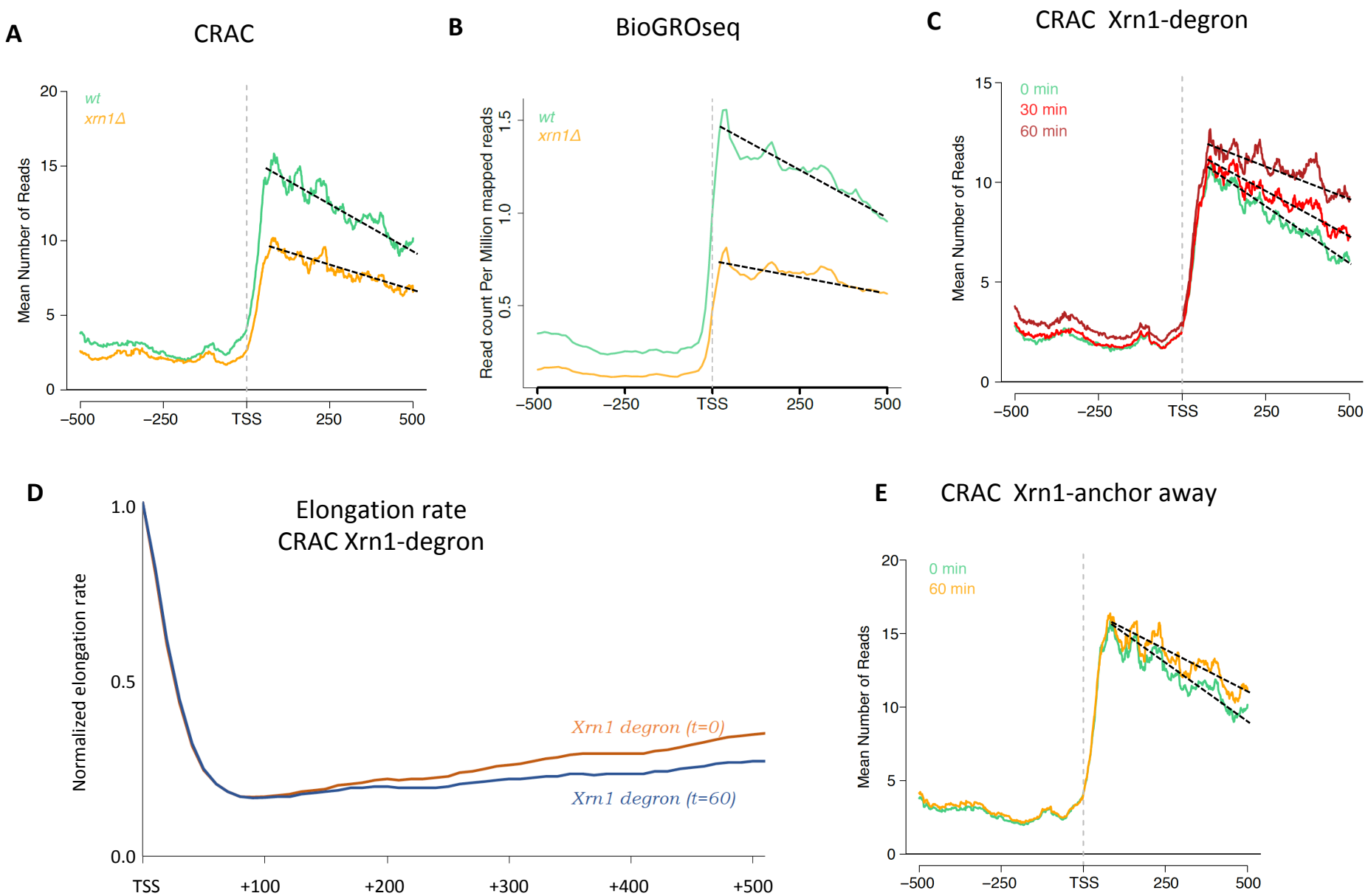
A
CRAC
wt
xrn1Δ
Mean Number of Reads
20
15
10
5
0
−500
−250
TSS
250
500
B
BioGROseq
wt
xrn1Δ
Read count Per Million mapped reads
1.5
1.0
0.5
−500
−250
TSS
250
500
C
CRAC Xrn1-degron
0 min
30 min
60 min
Mean Number of Reads
15
10
5
0
−500
−250
TSS
250
500
D
Elongation rate
CRAC Xrn1-degron
Normalized elongation rate
1.0
0.5
0.0
Xrn1 degron (t=0)
Xrn1 degron (t=60)
TSS
+100
+200
+300
+400
+500
E
CRAC Xrn1-anchor away
0 min
60 min
Mean Number of Reads
20
15
10
5
0
−500
−250
TSS
250
500

Figure 2

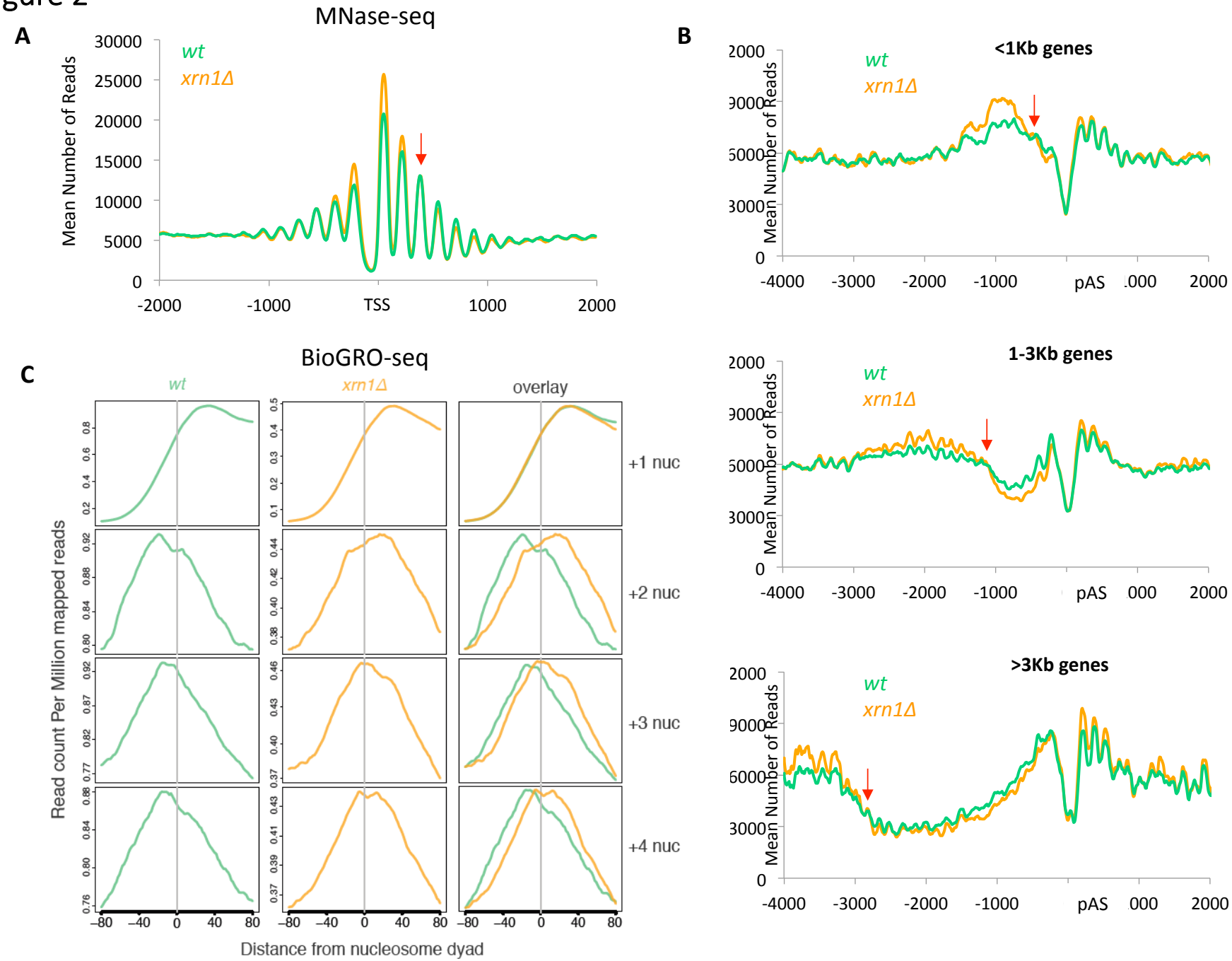
A
MNase-seq
wt
xrn1Δ
Mean Number of Reads
30000
25000
20000
15000
10000
5000
0
-2000
-1000
TSS
1000
2000
B
<1Kb genes
1-3Kb genes
>3Kb genes
Mean Number of Reads
-4000
-3000
-2000
-1000
pAS
2000
C
BioGRO-seq
wt
xrn1Δ
overlay
+1 nuc
+2 nuc
+3 nuc
+4 nuc
Read count Per Million mapped reads
Distance from nucleosome dyad

Figure 3

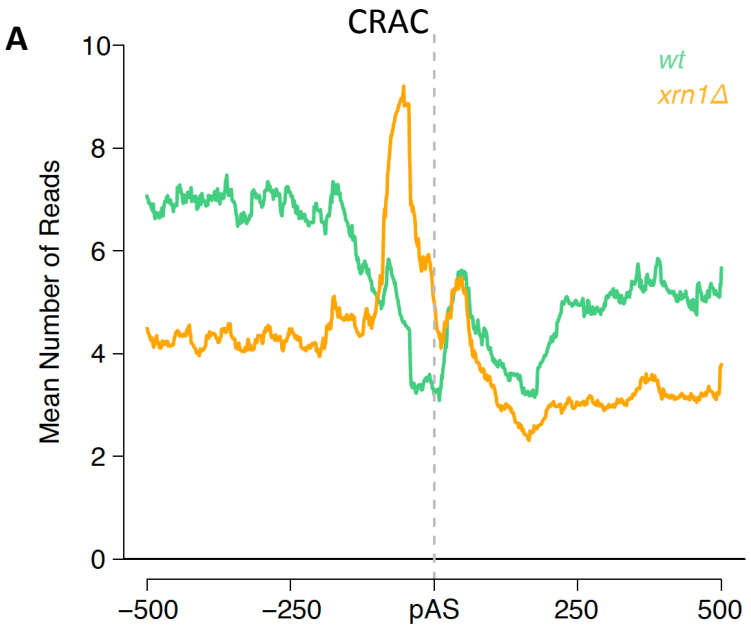
A
CRAC
wt
xrn1Δ
Mean Number of Reads
10
8
6
4
2
0
−500
−250
pAS
250
500

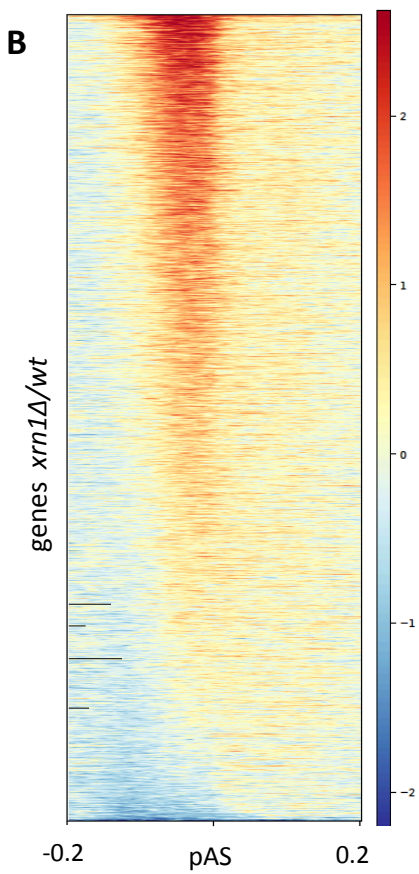
B
genes xrn1Δ/wt
-0.2
pAS
0.2

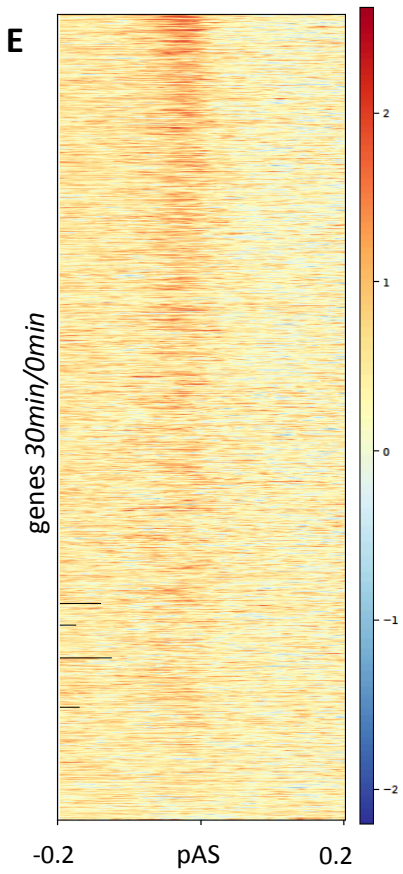
E
genes 30min/0min
-0.2
pAS
0.2

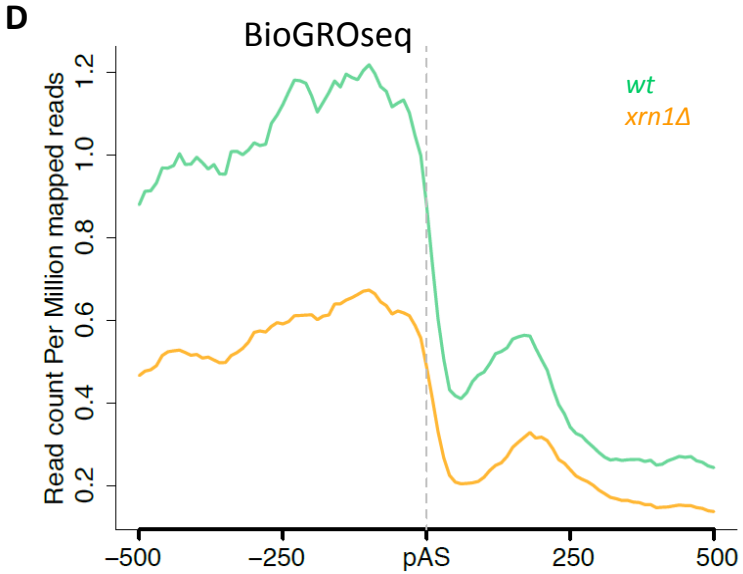
D
BioGROseq
wt
xrn1Δ
Read count Per Million mapped reads
1.2
1.0
0.8
0.6
0.4
0.2
−500
−250
pAS
250
500

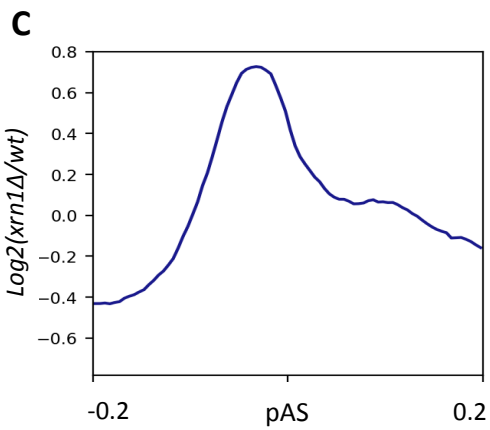
C
Log2(xrn1Δ/wt)
0.8
0.6
0.4
0.2
0.0
−0.2
−0.4
−0.6
-0.2
pAS
0.2

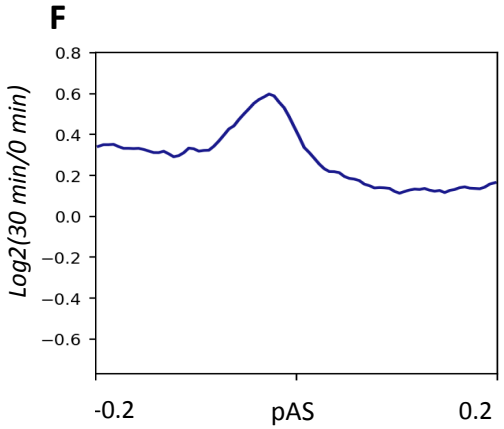
F
Log2(30 min/0 min)
0.8
0.6
0.4
0.2
0.0
−0.2
−0.4
−0.6
-0.2
pAS
0.2

Figure 4

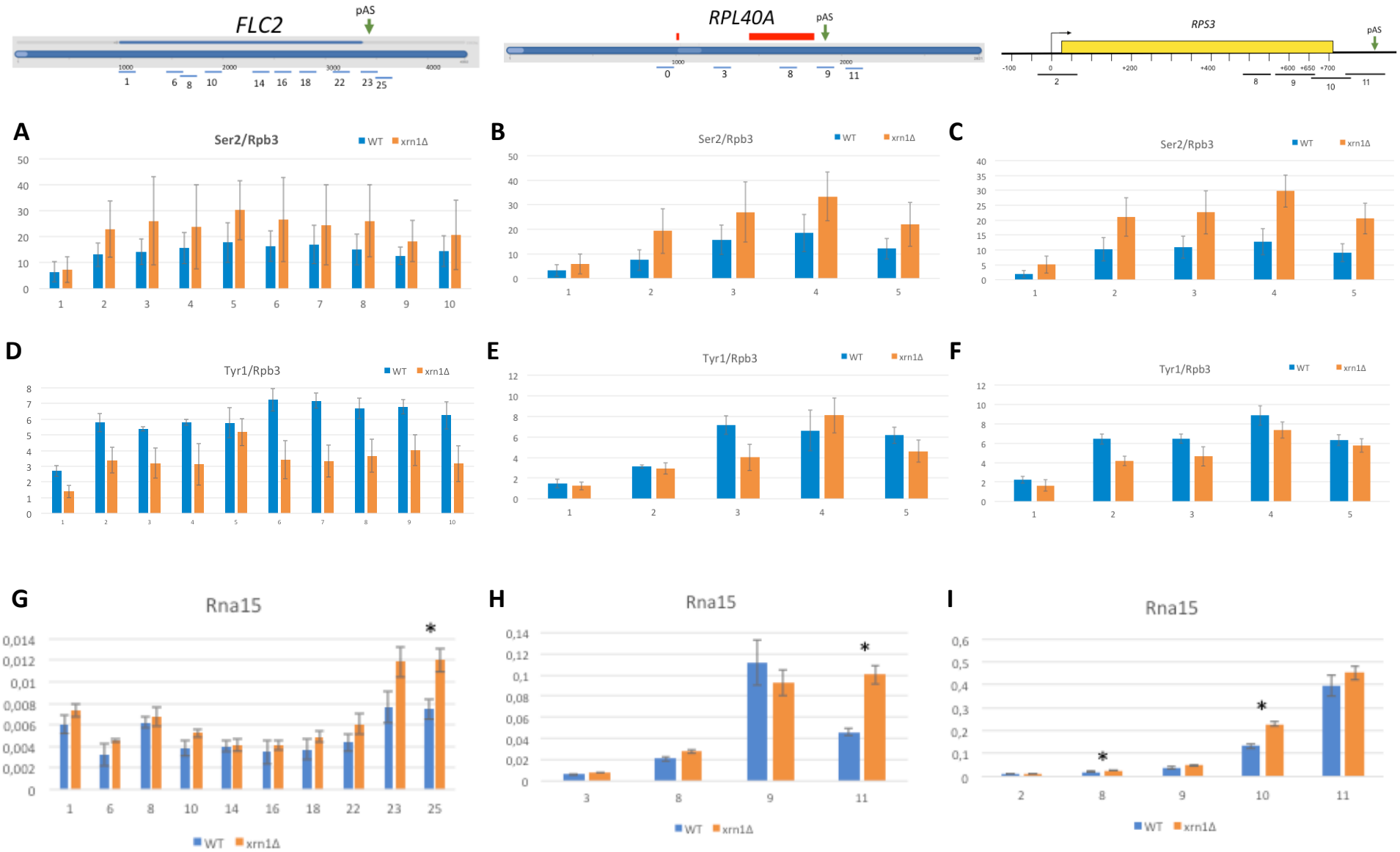
FLC2
pAS
RPL40A
pAS
RPS3
pAS
A
Ser2/Rpb3
WT
xrn1Δ
B
Ser2/Rpb3
C
Ser2/Rpb3
D
Tyr1/Rpb3
E
Tyr1/Rpb3
F
Tyr1/Rpb3
G
Rna15
H
Rna15
I
Rna15

Figure 5

A

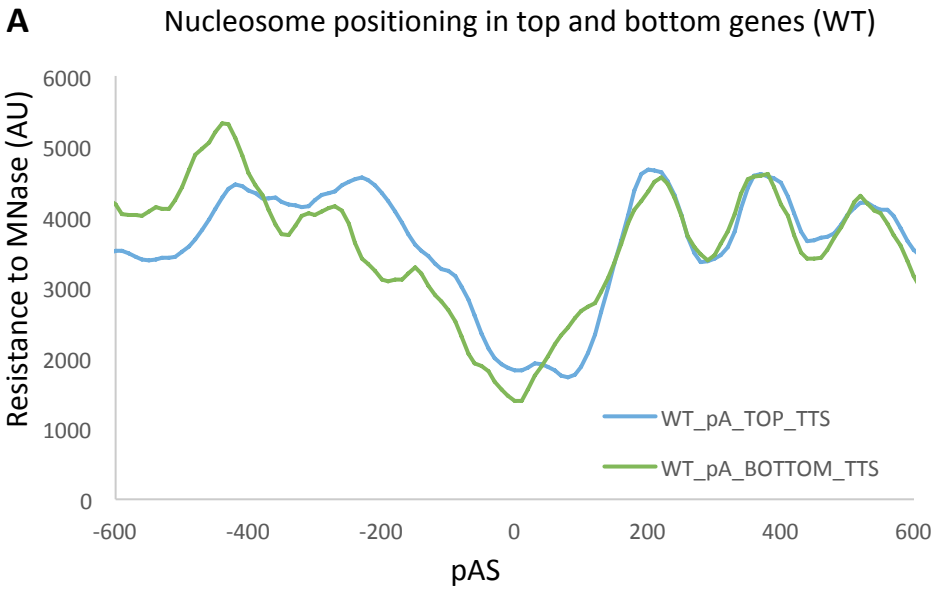

B

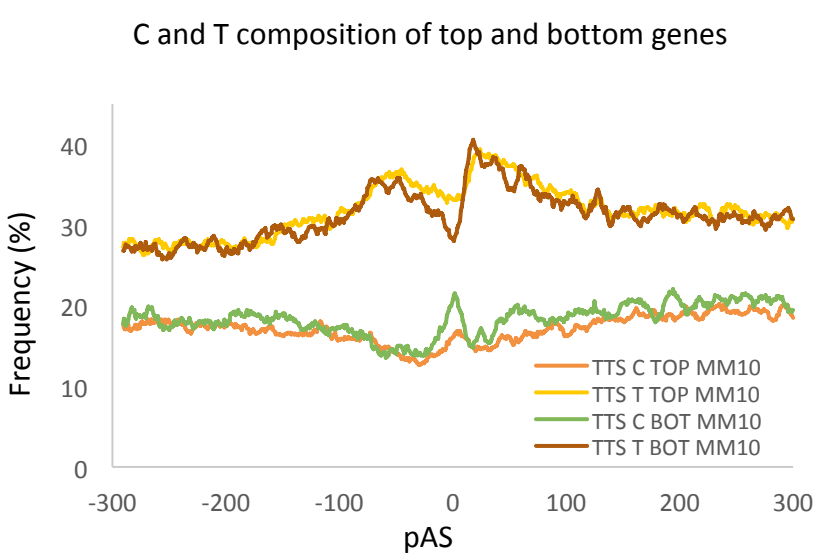

C

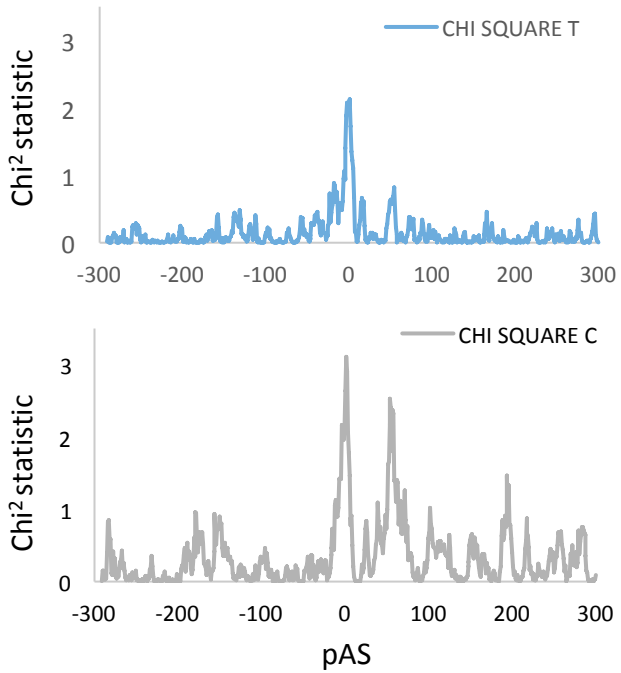

D

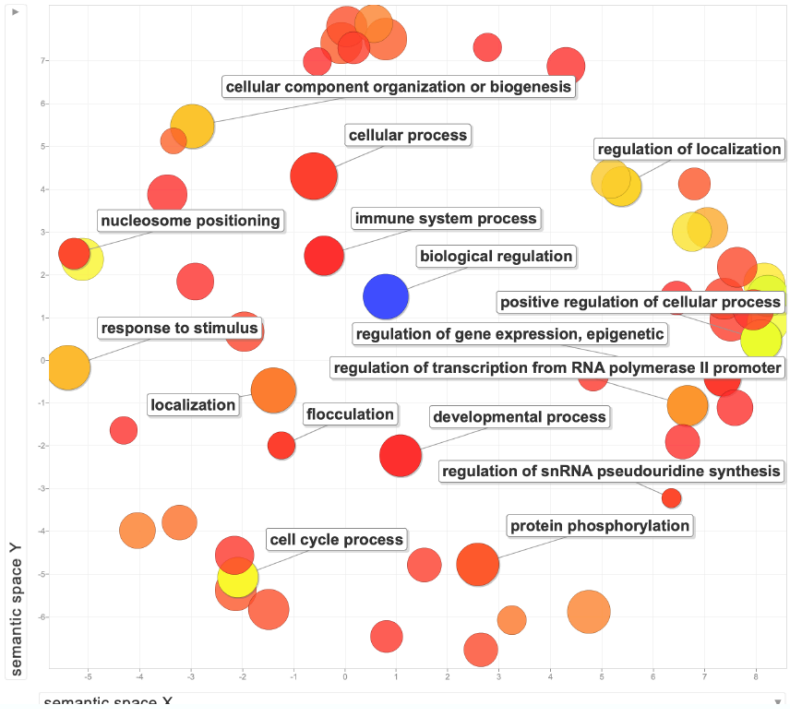

Figure S1

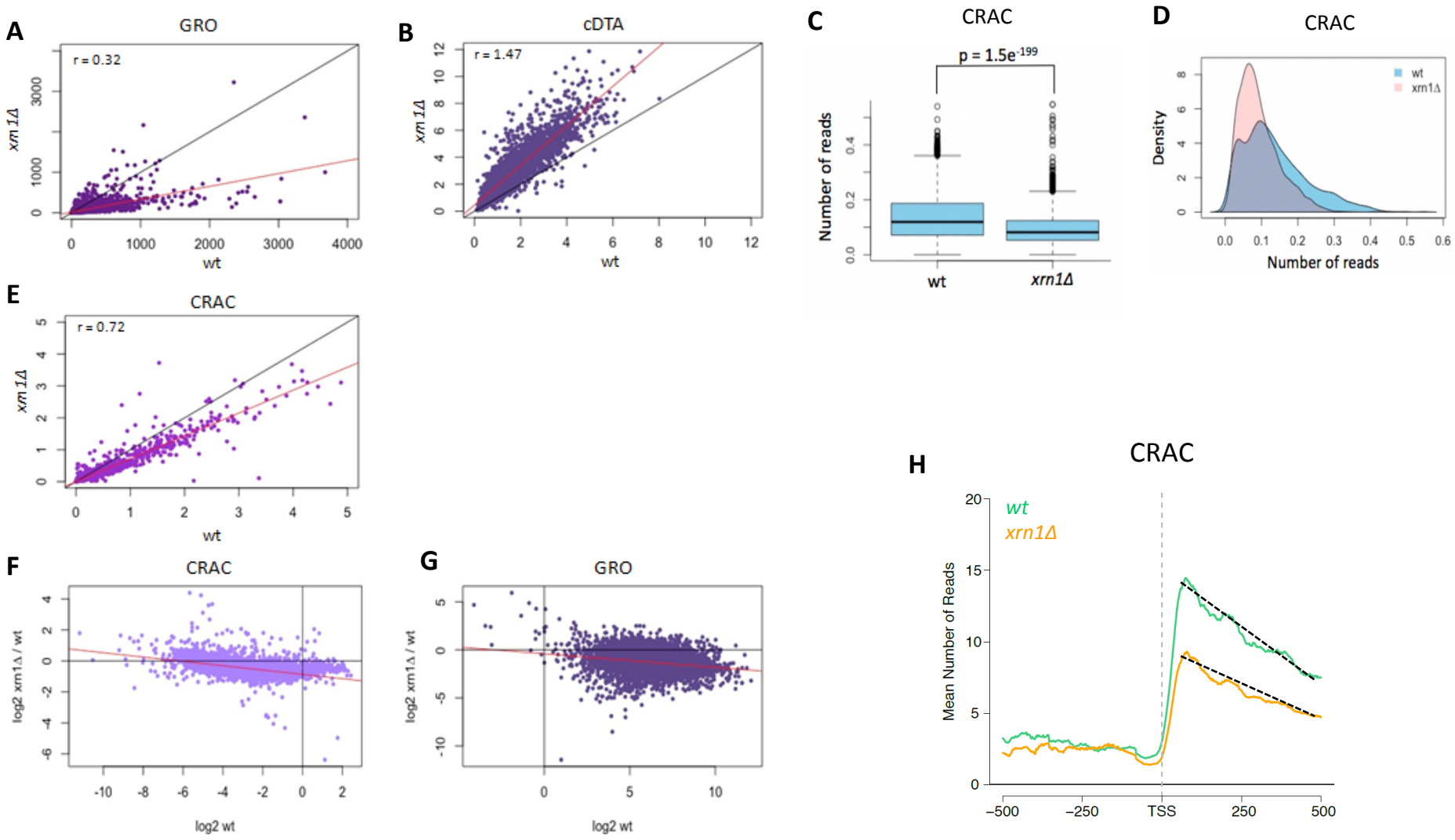
A
GRO
r = 0.32
xrn1Δ
wt
B
cDTA
r = 1.47
xrn1Δ
wt
C
CRAC
p = 1.5e-199
Number of reads
wt
xrn1Δ
D
CRAC
wt
xrn1Δ
Density
Number of reads
E
CRAC
r = 0.72
xrn1Δ
wt
F
CRAC
log2 xrn1Δ / wt
log2 wt
G
GRO
log2 xrn1Δ / wt
log2 wt
H
CRAC
wt
xrn1Δ
Mean Number of Reads
−500
−250
TSS
250
500

Figure S1. **The deletion of *XRN1* led to a reduction in transcription using the CRAC and GRO methods. A.** Scatterplot of the GRO data of *xrn1Δ* versus the wt. We can see a clear down-regulation of most genes in the mutant as represented by the red regression line. The r=0.32 represents the slope of this regression line. The black line shows where the data should align if the two datasets had the same values. If the dots are under this line, then transcription is down-regulated in the mutant with respect to the wt; and if they are above, then transcription is up-regulated. **B.** Scatterplot of the cDTA data obtained in Cramer's lab (Sun et al., 2013). Most genes are up-regulated in the mutant compared to the wt as shown by the red regression line, with a slope of 1.47. **C.** Boxplot representing the number of reads normalized to gene length for the wt and *xrn1Δ*. The black centre line represents the median of the number of reads (0.12 and 0.08 respectively). Then, reads are divided into quartiles. The box contains the reads from quartiles 2 and 3 (50% of all reads), and the whiskers show the quartile 1 (top whisker) and quartile 4 (bottom whisker). A two sample t-test shows that the differences are very significant ($p<0.005$) **D.** Density plot showing the density of reads versus the number of normalized reads. This represents how many times a read number appears in the data. **E.** Scatterplot of the CRAC data representing the number of normalised reads for the wt versus *xrn1Δ.* Most genes are down-regulated in *xrn1Δ* in comparison to the wt as represented by the red regression line with a slope of 0.72. **F,G.** Representation of the ratio between *xrn1Δ* and the wt versus the wt in both CRAC and GRO data. The effects are greater in highly transcribed genes.

Figure S2

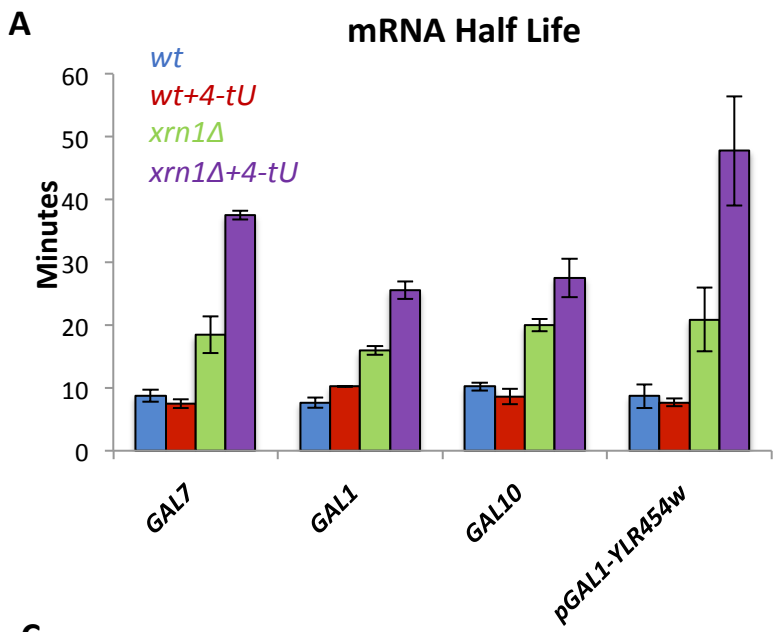
A
mRNA Half Life
wt
wt+4-tU
xrn1Δ
xrn1Δ+4-tU
Minutes
60
50
40
30
20
10
0
GAL7
GAL1
GAL10
pGAL1-YLR454w

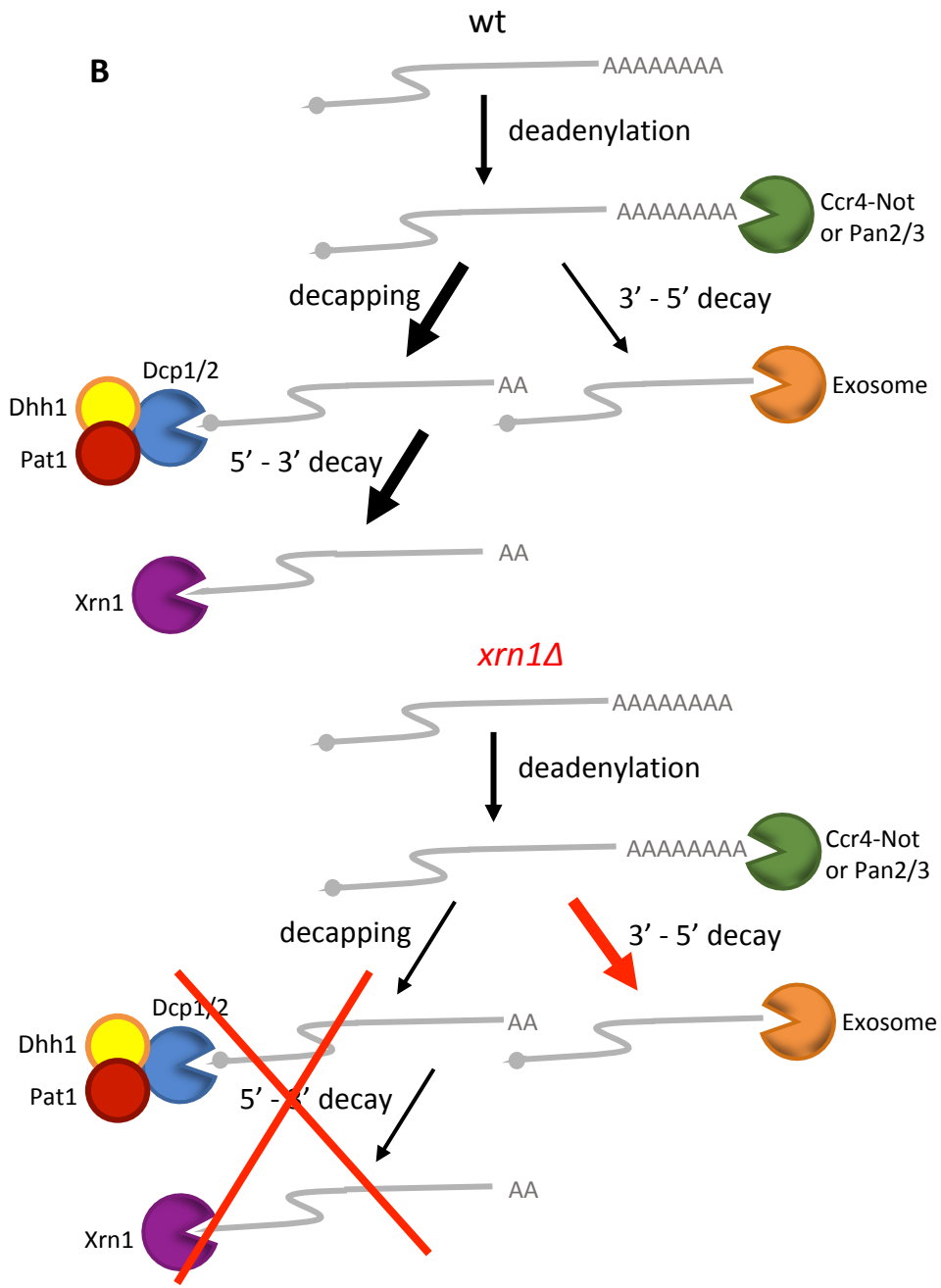
B
wt
AAAAAAAA
deadenylation
AAAAAAAA
Ccr4-Not
or Pan2/3
decapping
3' - 5' decay
Dcp1/2
Dhh1
Pat1
AA
Exosome
5' - 3' decay
AA
Xrn1
xrn1Δ
AAAAAAAA
deadenylation
AAAAAAAA
Ccr4-Not
or Pan2/3
decapping
3' - 5' decay
Dcp1/2
Dhh1
Pat1
AA
Exosome
5' - 3' decay
AA
Xrn1

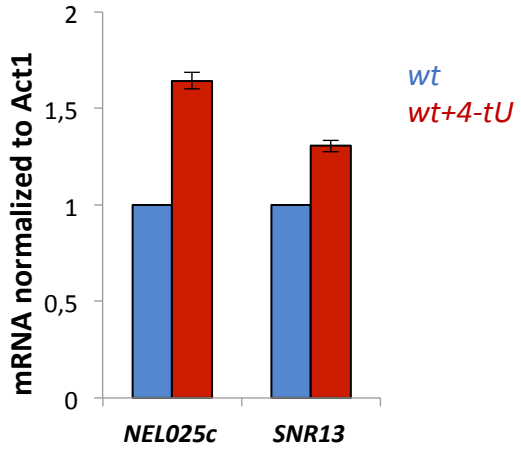
C
mRNA normalized to Act1
2
1,5
1
0,5
0
wt
wt+4-tU
NEL025c
SNR13

Figure S2. The use of 4-thiouracil (4-tU) leads to defects in degradation and transcription. A. Addition of 4-tU increases the mRNA half-life in an x*rn1Δ* strain. mRNA half-lives were estimated by using a transcriptional shut-off assay (see materials and methods), in a wt and x*rn1Δ* strain. Cells were grown to exponential phase and half of each type of cells were treated with 4mM 4-tU for 2 hours before performing the assay. mRNA signals were normalized to *SCR1*. The mean of two independent experiments are represented by bars. **B.** Scheme showing mRNA degradation pathways in yeast (adapted from Braun and Young, 2014). **C.** Addition of 4-tU leads to an accumulation of ncRNAs in a wild type strain. Cells were grown to exponential phase and half of the cells were treated with 4mM 4-tU for 45 minutes. RNA signals were normalized to *ACT1*, an mRNA that is not degraded by the exosome. The mean of two independent experiments are represented by bars.

Figure S3

CRAC

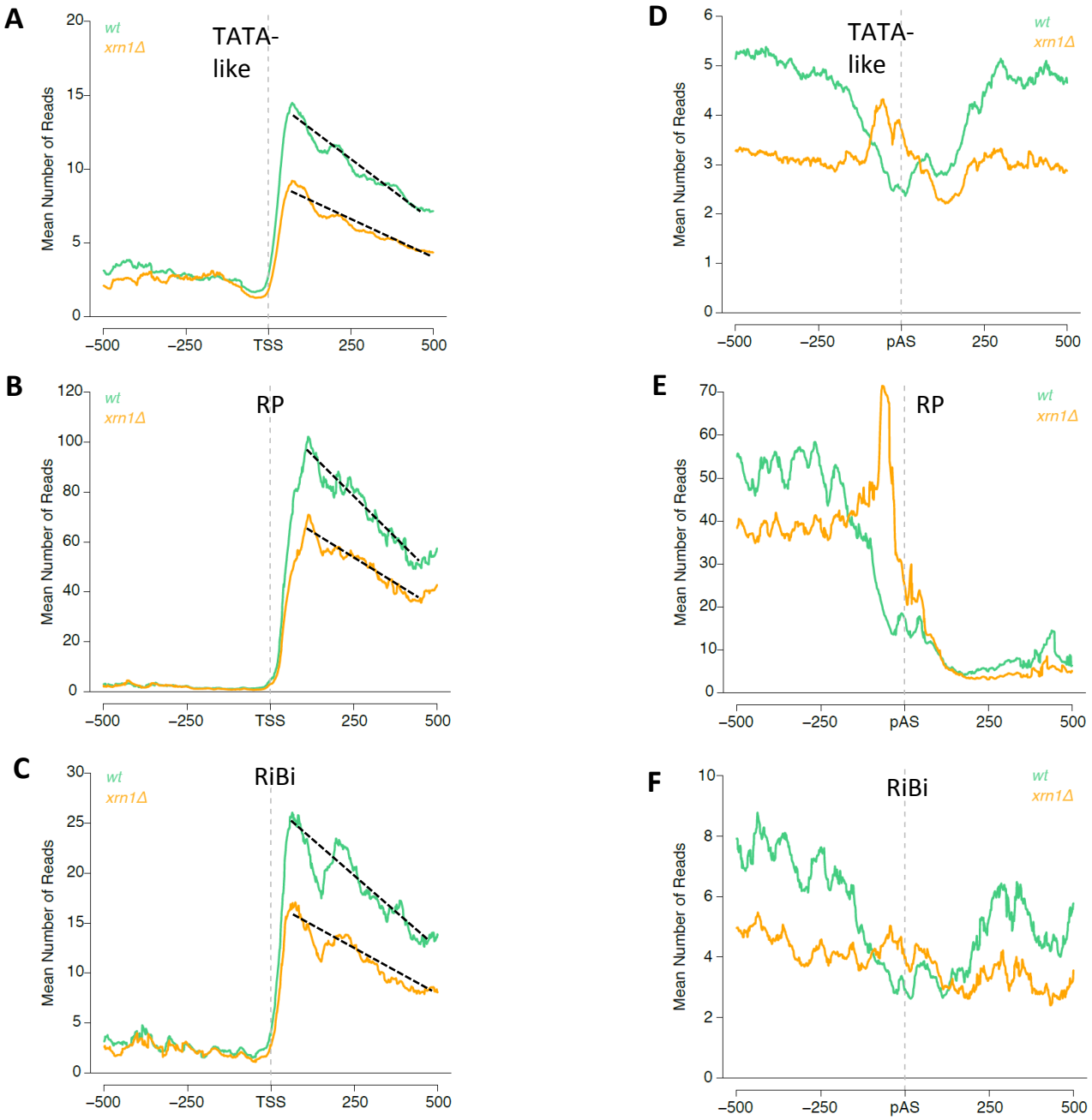

Figure S3. In other gene categories we can observe similar defects in *xrn1Δ* as for TATA genes. We divided the genes into four categories: TATA (TATA promoter containing genes - shown in figures 1A and 3A), TATA-like (TATA-like promoter genes, except for RP and RiBi genes), RP (ribosomal protein genes) and RiBi (ribosome biogenesis genes). On the left, we can find the CRAC-seq data aligned to the TSS (A-C) and on the right (D-F), to the pAS. The green lines represent the wt and the orange lines the *xrn1Δ*. In all types of genes there is a change in the slope from wt to mutant. The accumulation of RNApol II at the end of genes is very prominent in RP genes and detectable in TATA/like and RiBi genes.

Figure S4

CRAC

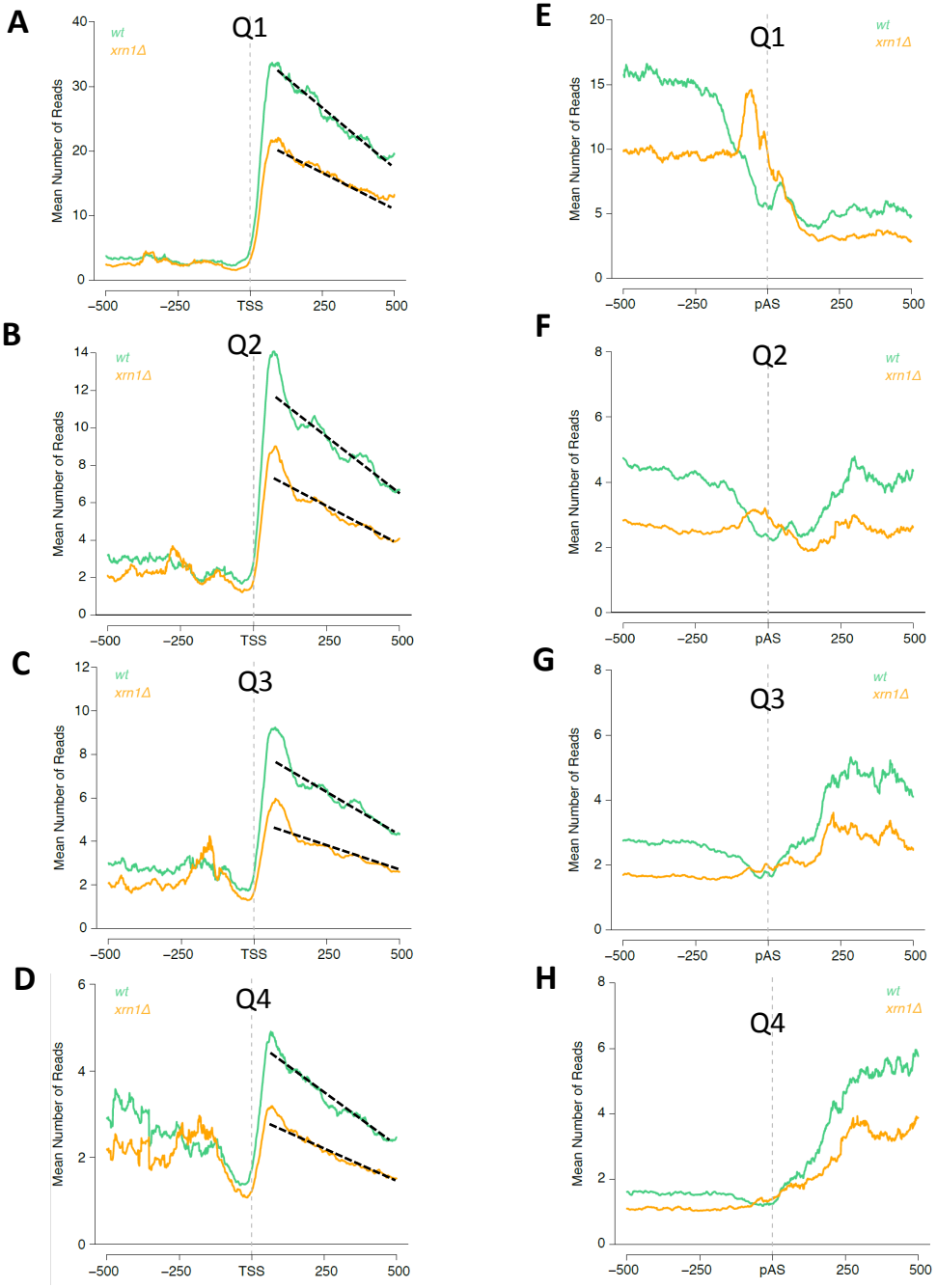

Figure S4. The late elongation defect is specific of highly expressed genes. We divided the genes based on their transcription levels measured by CRAC into quartiles. Q1 is the quartile with the highest expressing genes and Q4 the lowest. On the left (A-D), we can find the data aligned to the TSS and on the right (E-H), to the pAS. The green lines represent the wt and the orange lines the *xrn1Δ*. In all quartiles there is a change in the slope from wt to mutant. The accumulation of RNApol II at the end of genes is very prominent in Q1, visible in Q2, but disappears in Q3 and Q4.

Figure S5

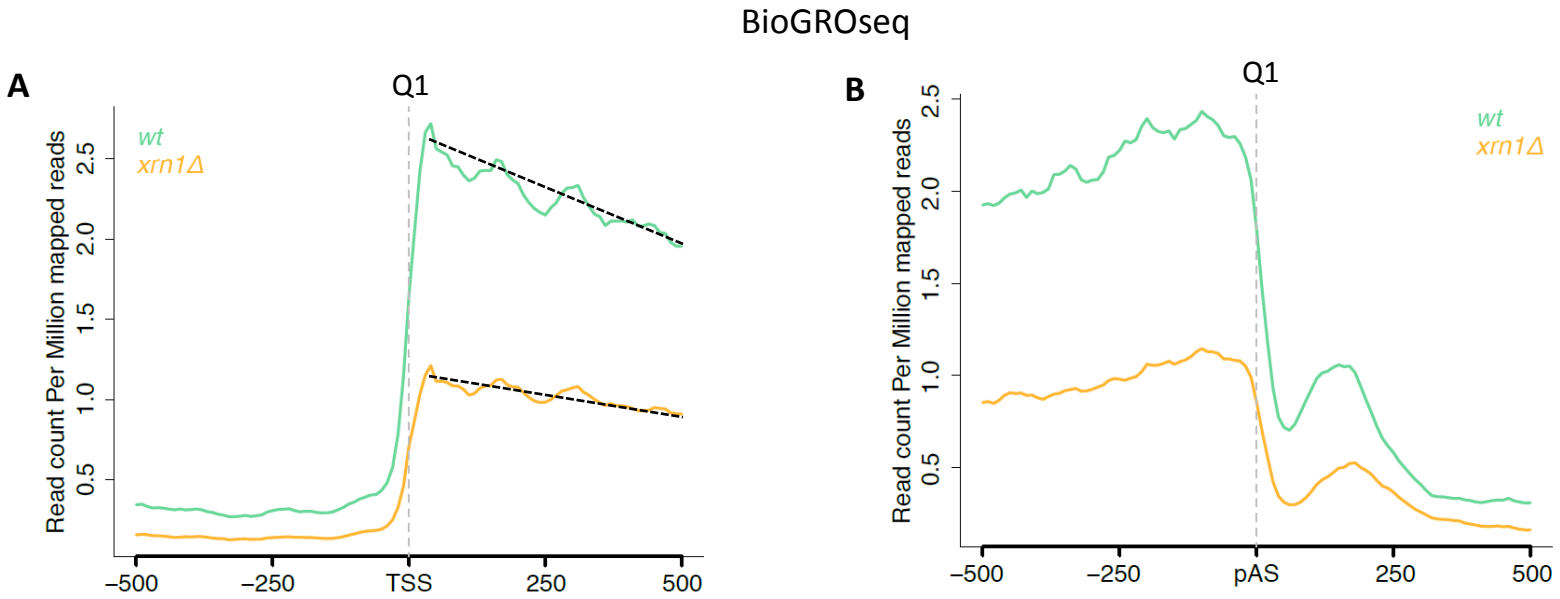

Figure S5. In the most highly transcribed genes we can observe the change in slope in the *xrn1Δ* mutant compared to the wt but no 3' end accumulation of active polymerases. We divided the genes based on their transcription levels measured by BioGRO (only active polymerases) into quartiles. Q1 is the quartile with the highest expressing genes. We plotted the genes relative to the TSS (A) or pAS (B). We found similar results as for the TATA gene group (figure 1B and figure 3D).

Figure S6

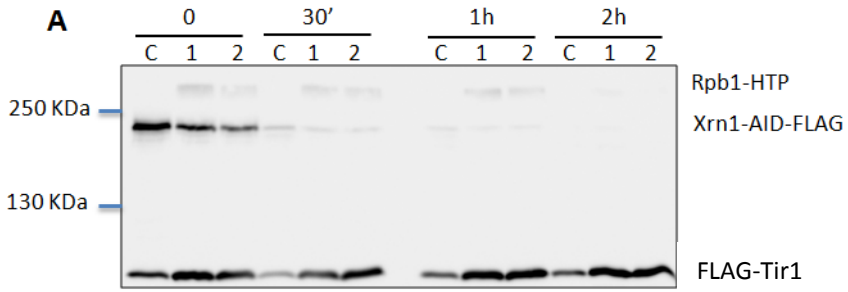

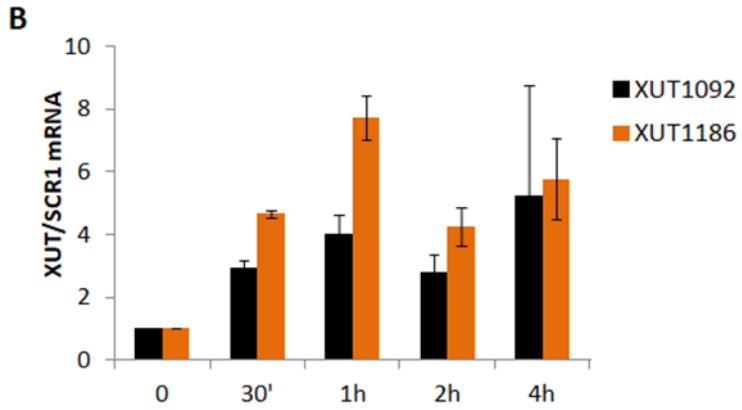

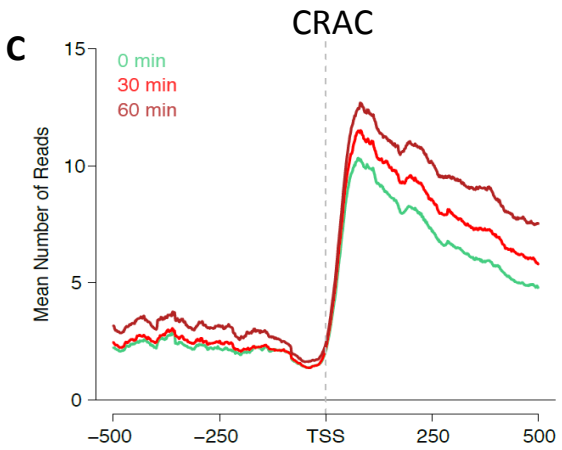

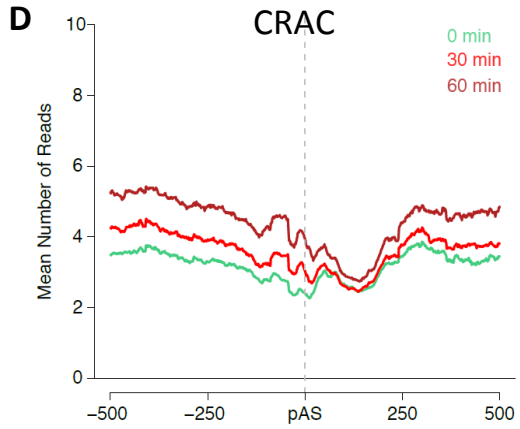

Figure S6. We successfully constructed a functional Xrn1-AID strain. A. Western blot showing the depletion of Xrn1-AID over time. The samples were obtained by growing cells to exponential phase and adding 0.2 mM of auxin and taking samples after the indicated times. The control strain, represented by a "C", is the BY4741 strain used to transform our W303 Rpb1-HTP strain. The numbers 1 and 2 represent two tested clones obtained from the transformation. We incubated our membrane with an anti-flag antibody that allowed us to see Xrn1 and Tir1 that we used as control of protein amounts. The secondary IgG antibody used allowed us to also see Rpb1-HTP in the clones. **B.** RT-qPCR shows an increase in the expression of two XUTs (defined in Wery et al., 2016) after auxin mediated depletion of Xrn1. From here on out we used clone 1 in our experiments. Bars represent the average of two separate experiments. From these experiments we determined that a depletion of 30 minutes and 60 minutes were the best times to use for further experiments. **C.** Metagene analysis of all genes detected with CRAC of Xrn1 auxin depletion aligned to the TSS. The green line shows the Xrn1-AID strain without auxin treatment (0 min) used as the control, and the red and dark red are with 30 min or 60 min of auxin treatment respectively. **D.** Same as in C but of all genes aligned to the pAS.

Figure S7

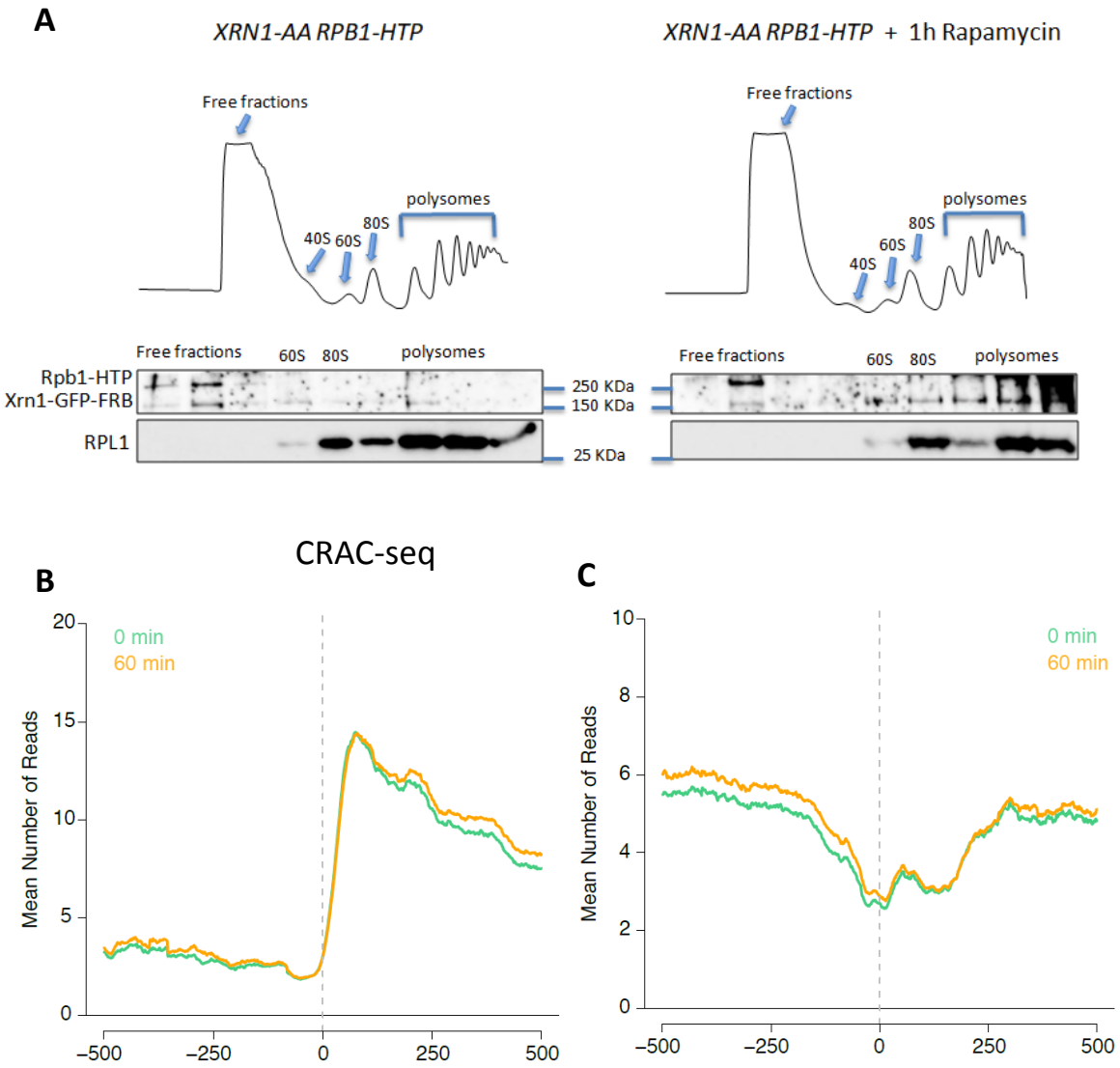

Figure S7. The Xrn1-AA strain is tethered to ribosomes upon rapamycin addition. We constructed the anchor away strain for our CRAC experiments from the strain used in Sun et al., 2013. A. Polysome profiles of the XRN1-AA RPB1-HTP strain with or without 1h rapamycin treatment. The fractions of these polysomes were collected and a western blot with the extracted protein was performed. We used anti-GFP to locate Xrn1, which also showed Rpb1-HTP, and anti-RPL1 to locate the RPL1 protein that assembles into the 60S ribosome subunit, 80S and polysomes. We show that without rapamycin, Xrn1 was mainly found in the free-fraction, and when rapamycin was added, Xrn1 was tethered to 60S ribosome subunits and polysomes. However, a part of the Xrn1 protein could still be found in the free fraction. B. Metagene analysis of Xrn1-AA aligning all genes to the TSS reveals early transcription elongation defects upon Xrn1 reduction in the nucleus. The green line shows the Xrn1-AA strain without rapamycin treatment (0 min) used as the control, and the orange line corresponds to 60 min rapamycin treatment. C. Metagene analysis of all genes aligned to the pAS.

Figure S8

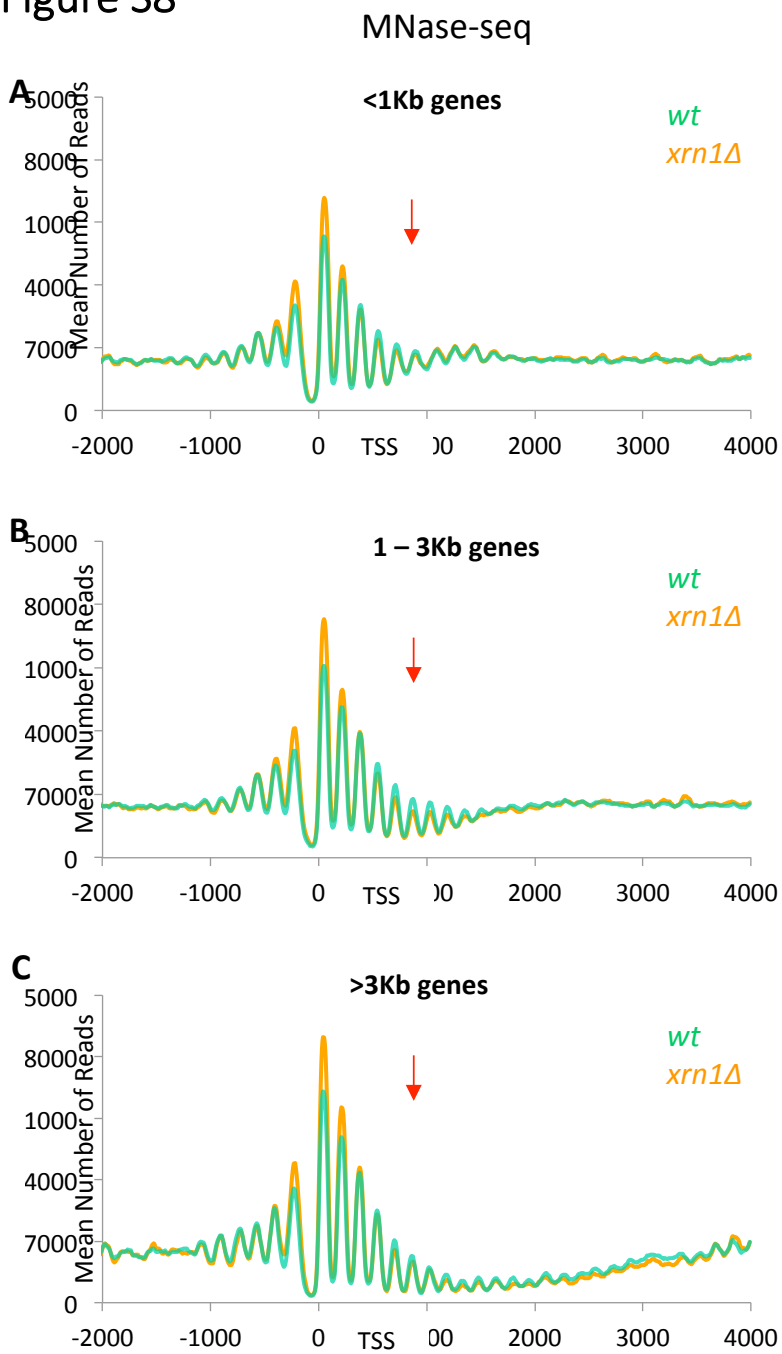

Figure S8. Changes in nucleosome occupancy was independent of gene length. We divided the genes by their length into three groups: less than 1 Kb (A), from 1 to 3 Kb (B) and longer than 3 Kb (C). We represented the nucleosomal maps of these genes aligned to the TSS. In green we show the wt and in orange *xrn1Δ.* As for all genes (Fig 2A), we detected in all cases a shift from higher nucleosome positioning to lower than the wt downstream of the +2 nucleosome. The red arrow indicates where the change occurs.

Figure S9

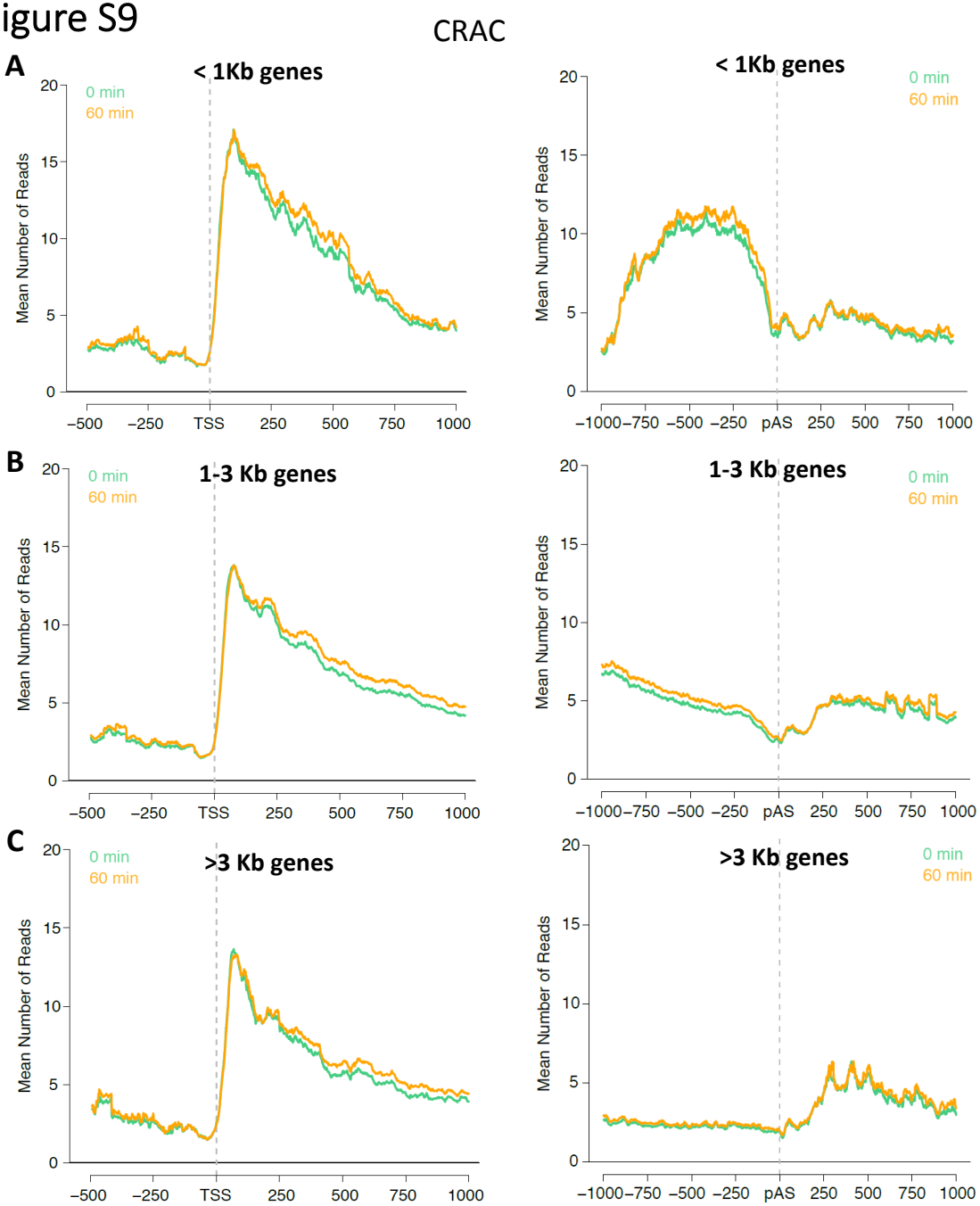

Figure S9. Metagene analysis of RNA pol II-CRAC data of Xrn1 AA experiment revealed as a function of gene length. The data used for Figure S7B were split into three groups according the length of their gene bodies (see Fig. 2B). A) Genes shorter than 1 kpb. B) Genes between 1 and 3 kbp long. C) Genes longer than 3 kpb. No important differences between wt and *xrn1Δ* mutant are seen for any gene length. In all cases the slope corresponding to the treated sample increased with respect to the wt in the 0-400 bp interval, and then the two continued in parallel.

Figure S10A

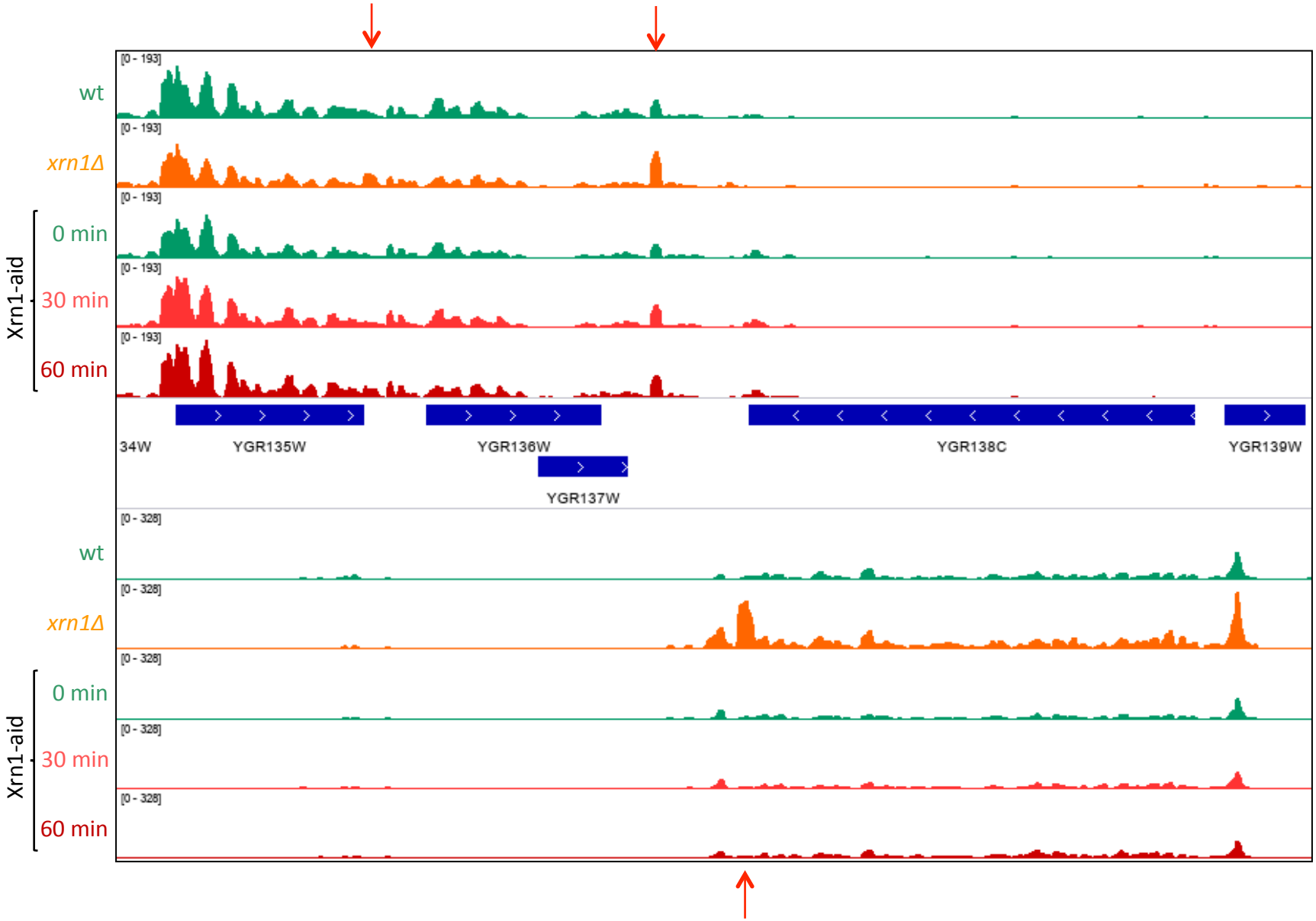
wt
xrn1Δ
Xrn1-aid
0 min
30 min
60 min
[0 - 193]
34W
YGR135W
YGR136W
YGR137W
YGR138C
YGR139W
[0 - 328]

Figure S10B

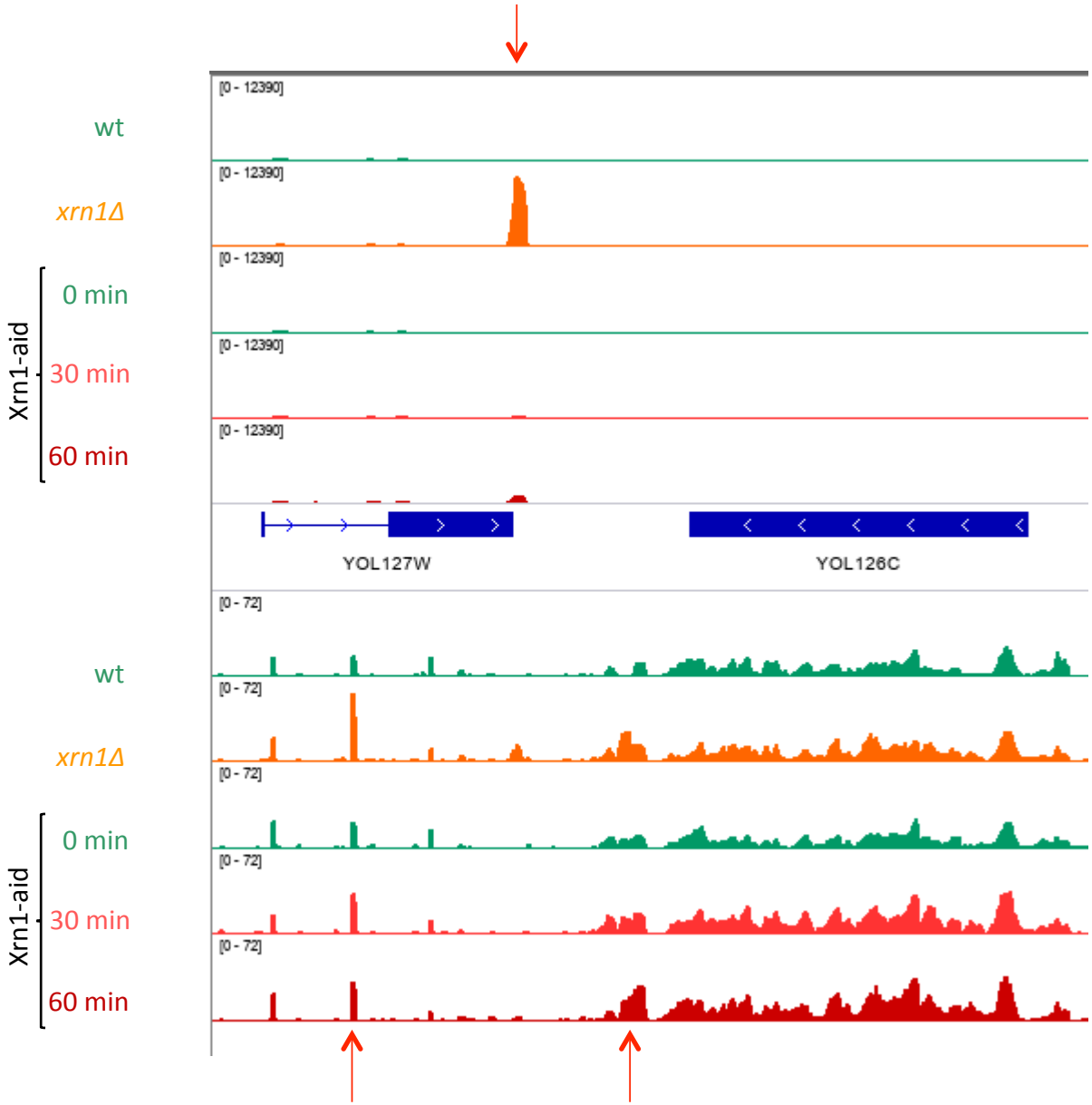
wt
xrn1Δ
Xrn1-aid
0 min
30 min
60 min
[0 - 12390]
YOL127W
YOL126C
[0 - 72]

Figure S10C

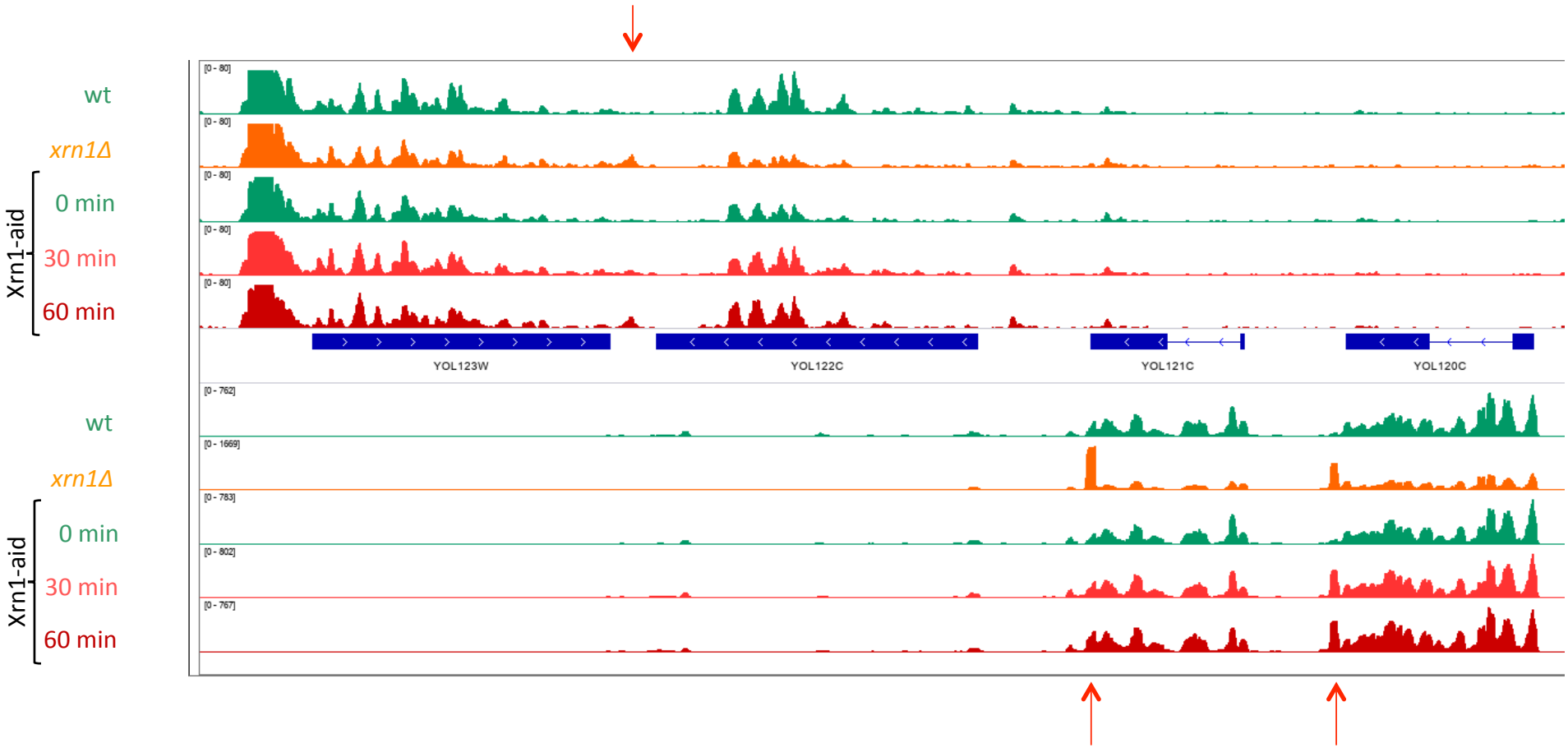

Figure S10. Several examples of genes showing RNApol II peaks at 3' in *xrn1Δ* and after depletion of Xrn1 by AID-degron.

Figure S11

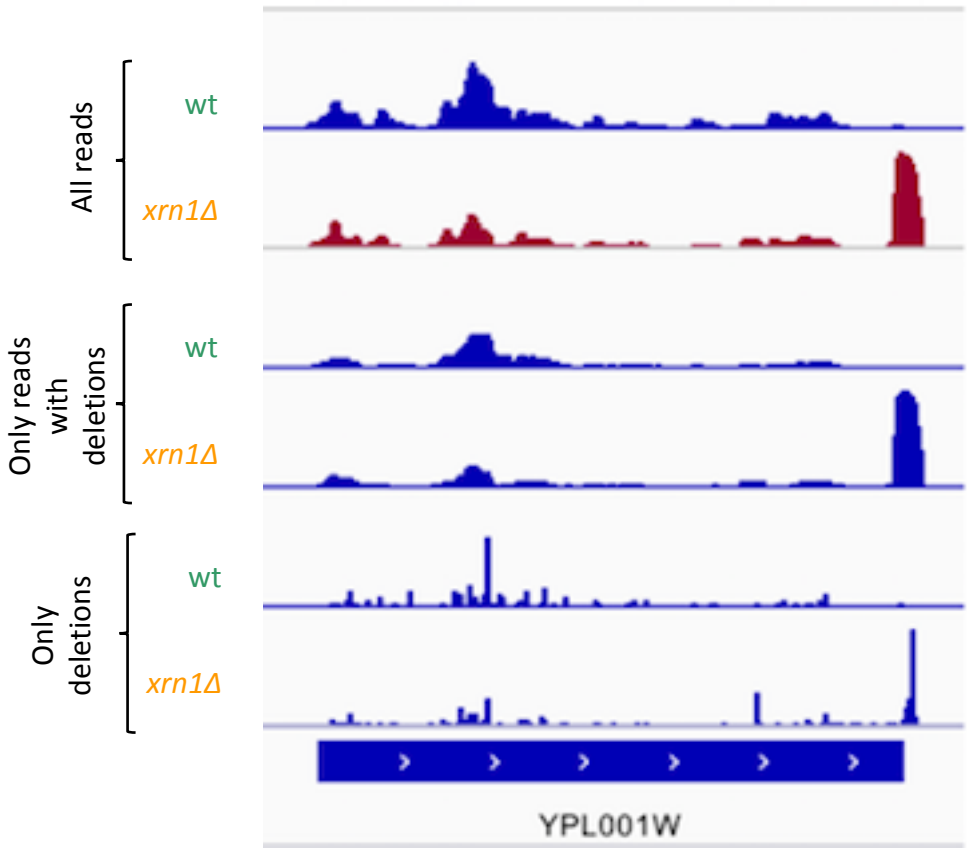

Figure S11. Deletion-containing reads confirm that 3' peaks are conformed by elongating RNApol II. all reads that contain a deletion (indicating the presence of a crosslink) were selected and a dataset containing only the position of the deletions (instead of the whole read) was generated. A genes showing a prominent peak of reads at 3' and the corresponding peak of deletions is shown.

Figure S12

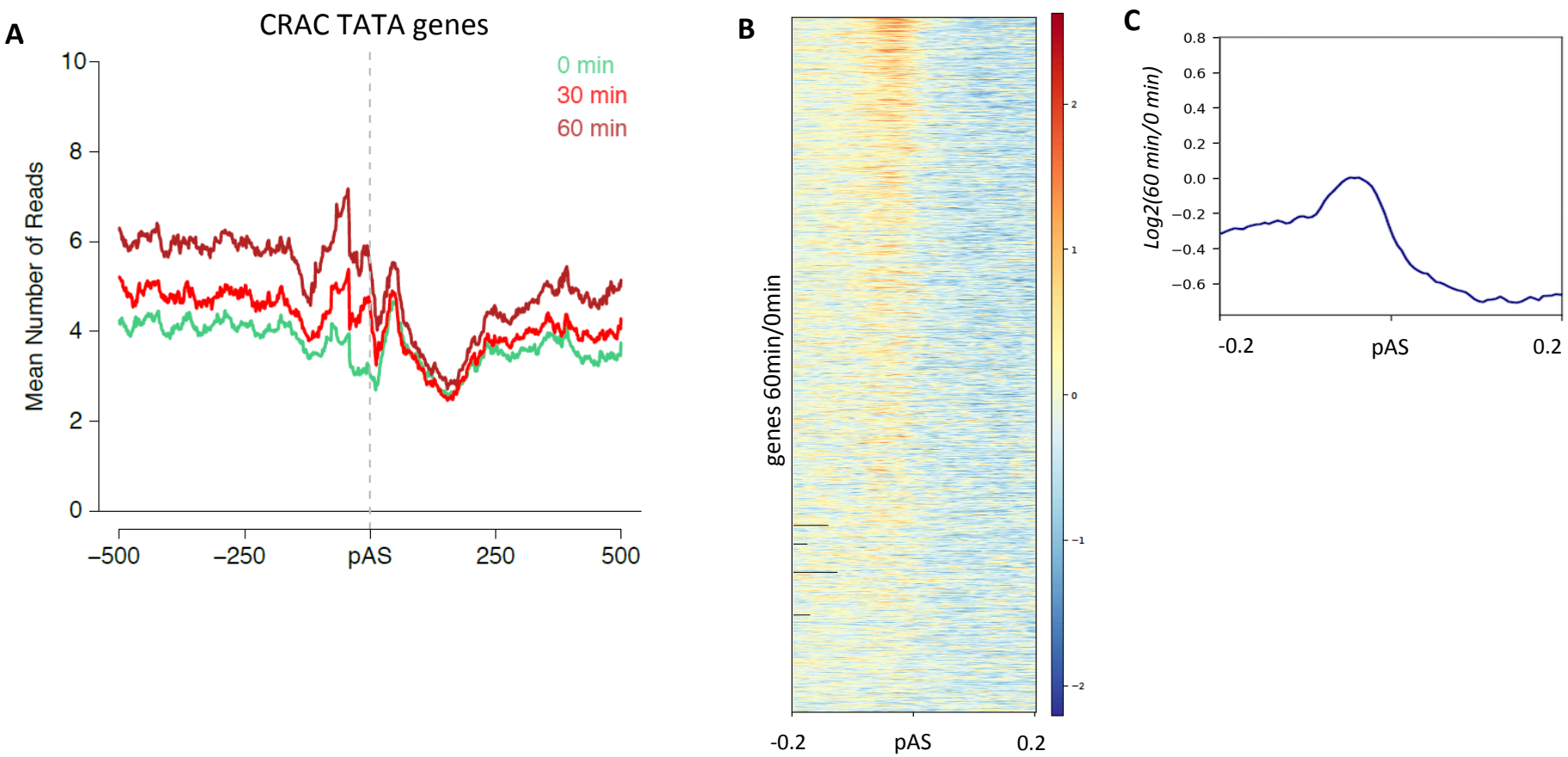

Figure S12. **Depletion of Xrn1 using the degron system produced an alteration of total RNA pol II profiles at the end of TATA-containing genes**. A. We found an increase in RNA bound to total RNA pol II measured by CRAC when depleting Xrn1 for 30 min (red) or 60 min (dark red) compared to the control (green) just before the pAS of genes. In this case we performed a metagene analysis of TATA containing genes and aligned the mean number of reads to the pAS with 500 bp either side of it. B. Heatmap of the Xrn1 depleted for 60 min data divided by the control data showing most genes present this increase in the amount of reads just before the pAS (in red). We show a +/- 200bp window from the pAS. Blue indicates lower reads, white no change, and in red higher amount of reads in the mutant versus the wt. C. Metagene representing the mean of what is shown in the previous heatmap.

Figure S13

ChIP-seq

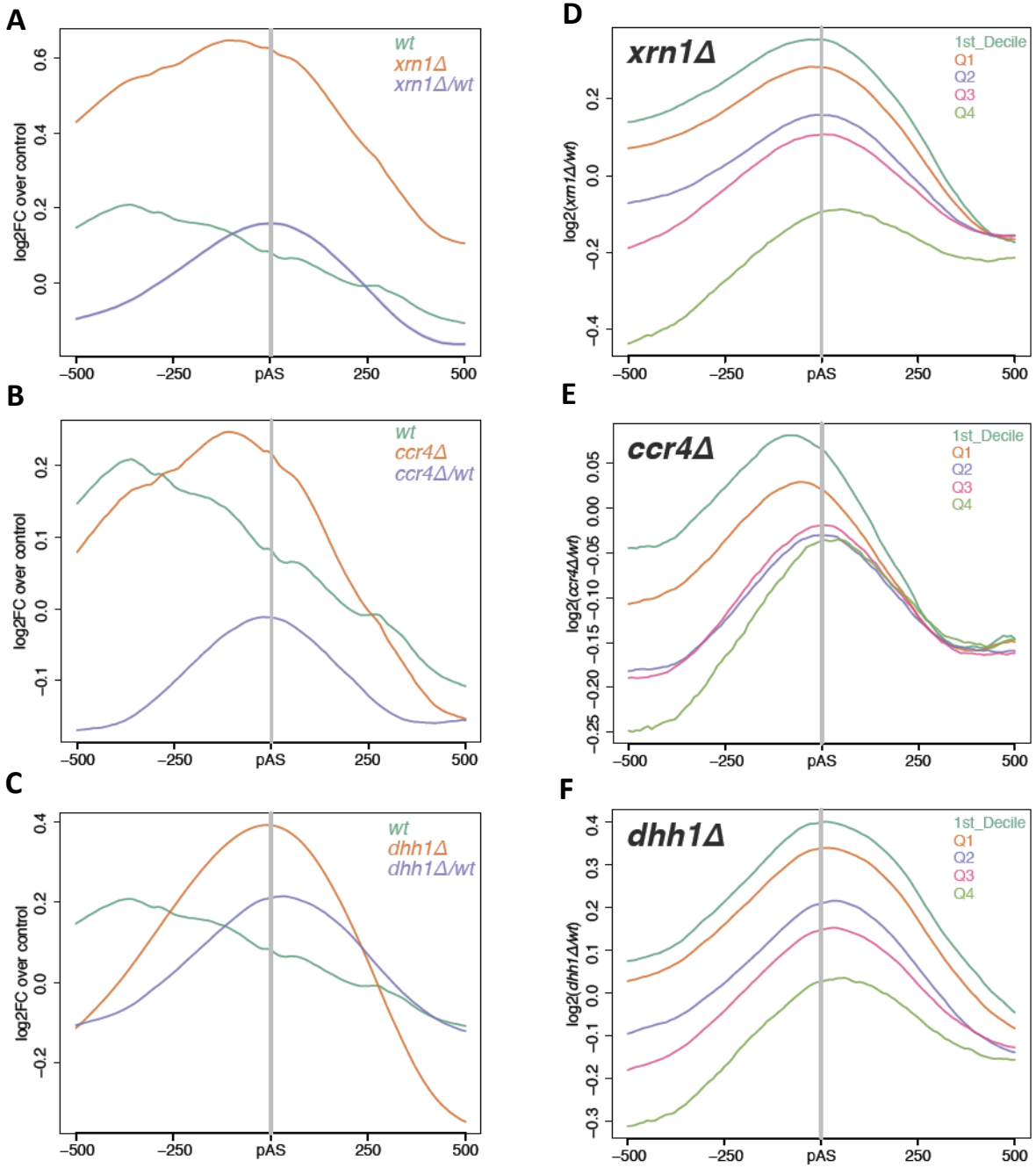

Figure S13. RNA pol II accumulates at the 3' end of genes in mRNA decay mutants. A) Metagene analysis of Rpb3 ChIP-seq in *xrn1Δ* versus wt shows an increased accumulation of RNA pol II at the 3' end of genes. In green we show the mean number of reads at each point of the wt (shown as IP/Input). In orange we see the result for *xrn1Δ*; and in purple we represent *xrn1Δ/*wt ratios. B-C) Metagene analysis of the Rpb3 ChIP-seq in *ccr4Δ* (B) and *dhh1Δ* (C) show similar results as for *xrn1Δ*. D-F) We show here the mutant/wt plots as in A-C but classifying the genes by their transcription rate. Decile 1 (D1) shows the top 10% of genes, quartile 1 (Q1) represents the genes with the highest signal and transcription rate, and quartile 4 (Q4) those with the lowest. The results show that the intensity of the pAS peak increases with the transcription rate.

Figure S14

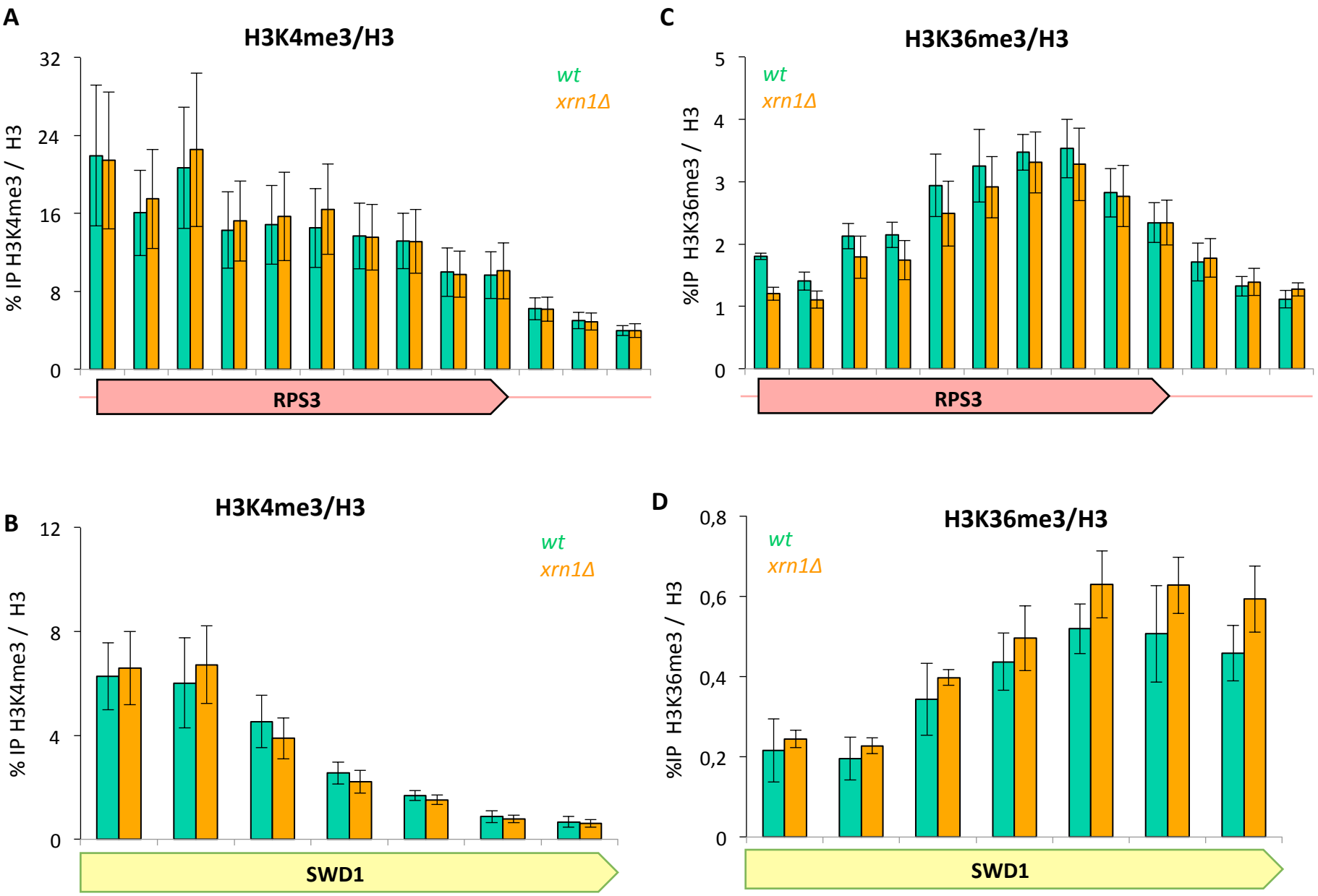
A
H3K4me3/H3
% IP H3K4me3 / H3
32
24
16
8
0
wt
xrn1Δ
RPS3
C
H3K36me3/H3
%IP H3K36me3 / H3
5
4
3
2
1
0
wt
xrn1Δ
RPS3
B
H3K4me3/H3
% IP H3K4me3 / H3
12
8
4
0
wt
xrn1Δ
SWD1
D
H3K36me3/H3
%IP H3K36me3 / H3
0,8
0,6
0,4
0,2
0
wt
xrn1Δ
SWD1

Figure S14. Changes in nucleosome patterns were not due to changes in histone modifications such as H3K4me3 and H3K36me3. A. No differences were found on the RPS3 gene between wt (green) and *xrn1Δ* (orange) in a H3K4me3 ChIP. the data was normalised to H3 to ensure changes were not due to changes in histone amounts, but in histone modifications (in this case methylation). B. No differences were found on the SWD1 gene between wt and *xrn1Δ* in a H3K4me3/H3 ChIP. C. No differences were found on the RPS3 gene between wt and *xrn1Δ* in a H3K36me3/H3 ChIP. D. No differences were found on the SWD1 gene between wt and *xrn1Δ* in a H3K36me3/H3 ChIP. In all cases the bars represent the mean values of three biological replicates.

Figure S15

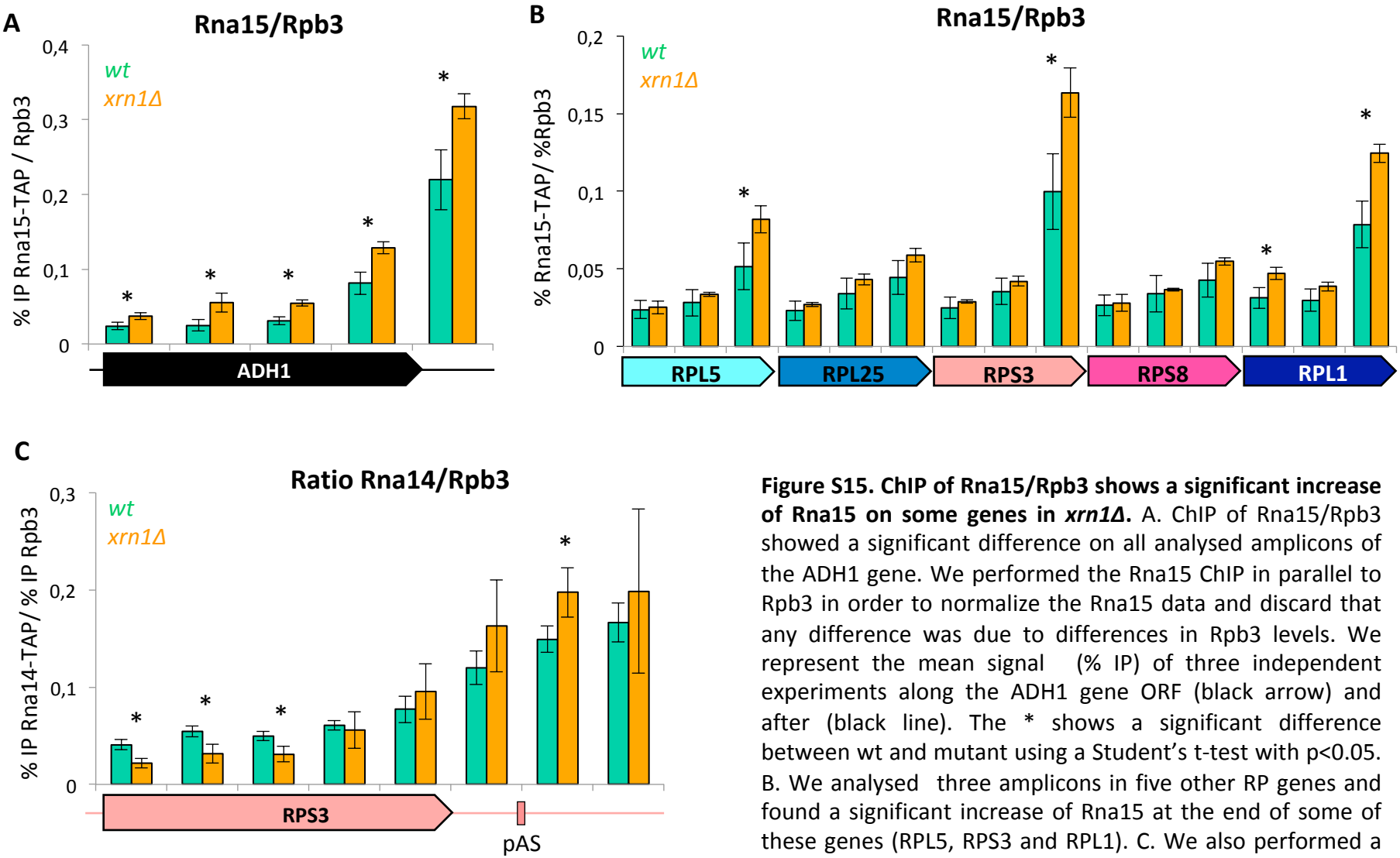

Figure S15. ChIP of Rna15/Rpb3 shows a significant increase of Rna15 on some genes in *xrn1Δ*. A. ChIP of Rna15/Rpb3 showed a significant difference on all analysed amplicons of the ADH1 gene. We performed the Rna15 ChIP in parallel to Rpb3 in order to normalize the Rna15 data and discard that any difference was due to differences in Rpb3 levels. We represent the mean signal (% IP) of three independent experiments along the ADH1 gene ORF (black arrow) and after (black line). The * shows a significant difference between wt and mutant using a Student's t-test with $p<0.05$. B. We analysed three amplicons in five other RP genes and found a significant increase of Rna15 at the end of some of these genes (RPL5, RPS3 and RPL1). C. We also performed a ChIP of Rna14 (a protein tightly associated to Rna15) and also found some differences in *xrn1Δ*.

Figure S16

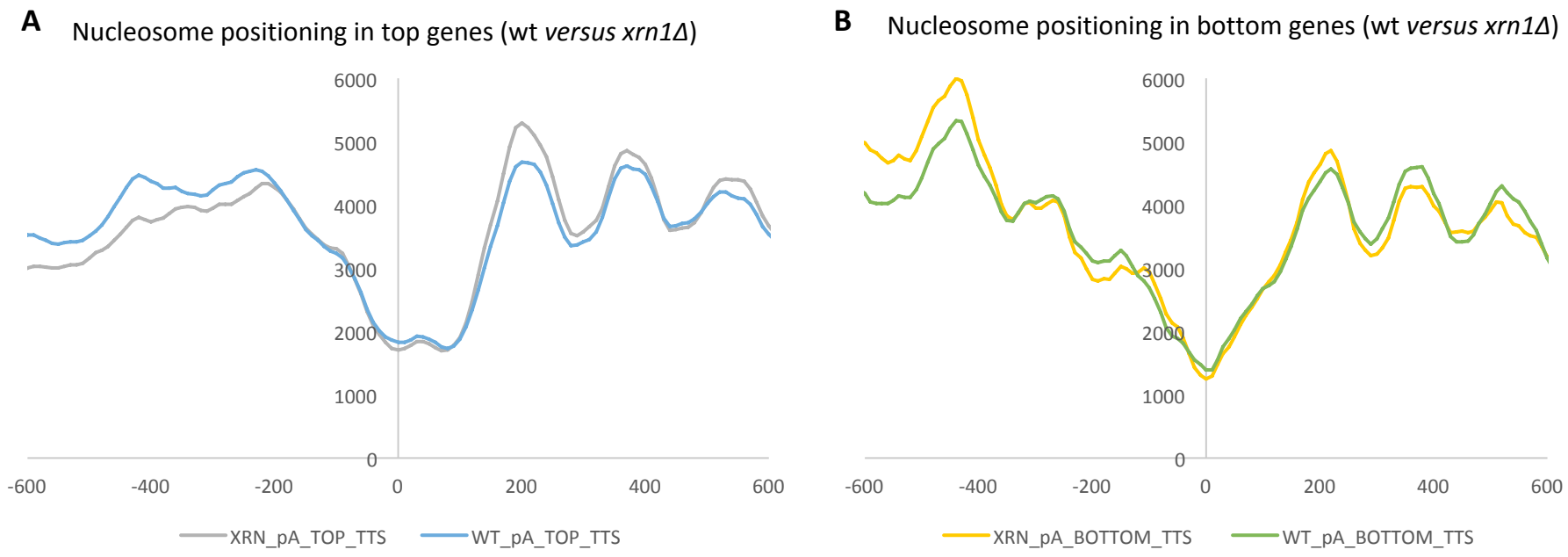

Figure S16. Nucleosomal patterns of top and bottom genes are not substantially altered by *xrn1Δ*. Maps of positioned nucleosomes of top (A) and bottom genes (B)around the pAS were obtained as an average of the patterns of resistance to MNase. Comparison of wt and *xrn1Δ* metagenes are shown.